UNIVERSITY OF CALIFORNIA

Santa Barbara

Changes in beach deposit characteristics on Joinville and Livingston Islands, Antarctica

A thesis submitted in partial satisfaction of the

requirements for the degree Master of Science

in Earth Science

by

Brittany Marie Theilen

Committee in charge:

Professor Alexander R. Simms, Chair

Professor Lorraine Lisiecki

Professor Vamsi Ganti

Professor Regina DeWitt, East Carolina University

December 2020

The thesis of Brittany Marie Theilen is approved.

_____

Lorraine Lisiecki

_____

Vamsi Ganti

_____

Regina DeWitt

_____

Alexander R. Simms, Committee Chair

December 2020

ACKNOWLEDGEMENTS

While the following thesis contains my small scientific contribution to the field of sedimentary geology, it cannot begin to describe the knowledge I have gained while in graduate school. I must begin by thanking my advisor, Dr. Alexander Simms, for reviewing and discussing my papers which helped me to become a better writer and researcher. Without his guidance and revisions, this thesis would not have been completed. Additionally, I am thankful for the funding provided by the National Science Foundation that gave me the opportunity to work on a MS project located in Antarctica.

My field expedition would not have been possible without the help of Cara Ferrier and Robin Carroccia in the field and the Lawrence M. Gould crew. Cara maintained our campsite on Livingston Island and cooked delicious meals each night while Robin was a great roommate aboard the LGM and was a tremendous field hand. I am thankful for their help in the field and having a chance to get to know both of these women.

I would also like to thank those who have helped me at UCSB. Firstly, I would like to thank Lorraine Lisiecki and Vamsi Ganti for serving as members on my committee. I appreciate the discussions on statistics, grain size, and research directions that steered me down the right path for this thesis.

I am very thankful for my lab mates, Julie Zurbuchen and Cameron Gernant for their help with data collection along the Antarctic beaches and office discussions. Julie completed most of the granulometry work on Joinville Island while Cameron was a great field partner and offered interesting discussion points regarding my results.

I am also thankful for Matt Rioux, Phil Gans, and Gareth Seward for helping identify ice rafted debris clasts from Joinville and Livingston Islands. I also cannot leave out the help of fellow graduate students Alex Johnson and Amy Moser. Amy showed me how to prepare and polish samples for the electron probe micro-analyzer for identification.

Additionally, I want to thank those who helped me at East Carolina University, Dr. Regina DeWitt and her PhD student Chris Garcia. I thank Dr. Regina DeWitt for serving on my committee and hosting me at East Carolina University for five weeks. I learned a lot about the process of optically stimulated luminescence dating on cobble surfaces and sliced many rock plugs. Dr. DeWitt was very helpful when I had questions about the OSL process and Chris Garcia was a great lab partner when working in the dark for 6+ hours.

Lastly, I would like to thank my family for all the emotional support they have provided me. To my parents, Troy and Amy, thank you for listening to me on the phone, and telling me how proud you both were of me. I could not have finished this thesis without you. To Joshua, thank you for being my rock during every step of the graduate school process, and listening to the same presentation dozens of times. To all the above, thank you for your support and encouragement, I truly could not have done this without you.

ABSTRACT

Changes in beach deposit characteristics on Joinville and Livingston Islands, Antarctica

By

Brittany Marie Theilen

The sedimentary characteristics of raised beach deposits are a potential archive of past wave climate as well as processes acting on beaches. In this study I examine changes in the grain-size, grain roundness, and spatial density of ice-rafted debris from two sets of raised beaches on opposite sides of the Antarctic Peninsula (AP): Joinville Island along the Eastern AP (EAP), and Livingston Island along the Western AP (WAP). All beaches were labeled starting at the closest proximity to the modern shoreline. Overall, the 9 beaches on Livingston Island are stratified with poorly sorted clasts compared to the better sorted 21 stratified lower beaches and 15 unstratified upper beaches on Joinville Island. The dissimilarity likely reflects the difference in foreshore gradient between the two islands. The Joinville profile is steeper, allowing waves to break on the coastline with high energy while the Livingston profile is shallower, enabling wave attenuation before reaching the shoreline. Grains on the raised beaches of Joinville Island show an overall increase in roundness through time while grain size shows low variability. However, the roundness trend is interrupted at beaches 5, 13-15.5, and 28. Beach 5 exhibits less and beach 28 exhibits more rounding than the general trend. Less rounding of sediments within beach 5 could be

explained by short open water seasons with an increase in sea ice while the opposite could hold true for beach 28. The transition between beaches 13 and 15.5 indicates a decrease in roundness over time, opposite the overall roundness trend. The ages of beaches 15.5-13 (~2.8-2.3 cal. kyr BP) coincides with the onset of the Neoglacial time period ~3 cal. kyr BP. The presence of sea-ice or increased glacial activity could hinder clast rounding or introduce less rounded materials during cooler periods associated with this Neoglacial time period. Grains within Livingston Island beach ridges also show an overall increase in roundness through time but no coherent trends in grain size. However, Livingston Island contains two types of beach deposits: strand plains and beach ridges, the latter of which are interpreted as storm ridges. Strand plains were deposited by normal swash processes and exhibit sub-angular to sub-rounded sediments. Typically, storm ridge sediments would be less rounded, characteristic of high energy storm deposits, than the strand plain deposits, roundness and grain size are uncorrelated. However, the beach ridges contain sub-rounded to rounded deposits while the strand-plain deposits are sub-angular to sub-rounded. Ground penetrated radar profiles through the beach ridge crests suggest they bury older strand-plain deposits. Therefore, I suggest the more rounded nature of the beach ridge deposits on Livingston Island is due to the recycling of older strand-plain deposits by storms.

TABLE OF CONTENTS

LIST OF FIGURES

LIST OF TABLES

1. Introduction

The Antarctica Peninsula is one of the fastest warming locations in the world (Vaughan et al., 2003). Late Holocene paleoclimate data are crucial for placing these observations of modern, rapid warming in context. Holocene climate events across the AP are recorded in high resolution marine and ice core records (Domack, 2002; Michalchuk et al., 2009; Milliken et al., 2009; Mulvaney et al., 2012). Proxy data from marine, ice, and lacustrine cores record past periods of warming and cooling driven by wind shifts, ocean circulation changes, and El Niño-Southern Oscillation (ENSO) variability (Barbara et al., 2016; Domack et al., 2001; Shevenell et al., 2011). However, one underutilized paleoclimate proxy is the sedimentary characteristics of beach deposits (Scheffers et al., 2012; Simkins et al., 2015), which along most Antarctic coastlines have been uplifted and thus preserved due to post-glacial rebound. Because these beach deposits reflect coastal environmental characteristics such as wave climate, sea-ice cover, and iceberg density (Hall and Perry, 2004; Simkins et al., 2015), changes in their characteristics may reflect environmental changes through the Holocene.

Wave climate provides a first order control on beach deposit characteristics (Butler, 1999). High magnitude, low frequency storm events are thought to be responsible for building coarse clastic beach ridges (Baroni and Hall, 2004; Butler, 1999; Carter and Orford, 1984; Forbes et al., 1995; Gardner et al., 2006; Hall, 2010; Lindhorst and Schutter, 2014; Simkins et al., 2015; Tamura, 2012) while normal swash processes, associated with lower wave energy, deposit strand plain sediments characterized by finer grain sizes (Lindhorst and Schutter, 2014). Any changes in the relative importance of storm events and normal swash

processes may be reflected in the temporal record of beach ridge versus strand plain development.

In addition to the type of beach developed, granulometry has also been used as a proxy of wave conditions across the Antarctic Peninsula (Bentley et al., 2005a; Simkins et al., 2015). The presence of sea ice restricts wave exposure and sediment supply to the beach (Butler, 1999; Nichols, 1961) by limiting fetch, thus decreasing wave energy. Therefore, in the absence of fluvial processes within Antarctica, cooler conditions associated with sea ice and the less frequent reworking of beach cobbles are thought to be characteristic of beach deposits with more poorly rounded clasts (Butler, 1999; Nichols, 1961; Simkins et al., 2015). Warmer conditions associated with no sea ice and higher wave energy are thought to be characteristic of beach deposits consisting of more rounded clasts (Nichols, 1961).

Additionally, the presence or absence of sea ice will affect ice rafted debris (IRD) counts and the internal sedimentary architecture of beach ridges. Hall and Perry (2004) used IRD on Byers Peninsula of Livingston Island in the South Shetland Islands (SSI) to create a climate proxy for the northern AP during the Holocene. The proxy is based on IRD densities from boulder counts along the beach ridges. Higher IRD counts were interpreted to represent cooler climate conditions marked by glacial advances (Hall and Perry, 2004) while low IRD counts represent warmer conditions and glacial retreat (Kanfoush et al., 2002).

The purpose of this study is to characterize trends in grain-size, clast roundness, and IRD on raised beach deposits through the late Holocene on Joinville and Livingston Islands along the EAP and WAP, respectively. Changes in these proxies through time are hypothesized to reflect changes in processes operating on beaches through the late Holocene. This archive will also augment studies of paleo sea levels derived from raised beaches by

providing a background to what other changes may be responsible for beach ridge elevation changes. My central hypothesis is that the sedimentary characteristics of Joinville beaches will record changes in wave climate through time while Livingston Island beaches will simply reflect differences between the two types of beach deposits found on the island.

2. Background

2.1 Modern Climate and Oceanographic Setting

The mountains located along the AP act as a barrier for winds and ocean currents between the WAP and the EAP. The Antarctic Circumpolar Current (ACC) causes upwelling of warm Circumpolar Deep Water (CDW) associated with warming along the WAP margin (Bentley et al., 2009; Hofmann et al., 1996). Additionally, the Southern Westerly wind belt is influenced by sea surface temperature gradients within the ACC (Manabe and Stouffer, 1997), the position of the southeast Pacific anticyclone and circum-Antarctic low pressure belt (Bentley et al., 2009), and Southern Annular Mode (SAM) events (Moreno et al., 2018). Models suggest the poleward shift in the Southern Westerly wind belt observed over the last 40 years is a response to anthropogenic warming (Shindell and Schmidt, 2004). Therefore, these latitudinal shifts impact the position of the ACC.

Conversely, the EAP is subjected to colder, more saline Weddell Sea Transitional Waters (WSTW) from the Weddell Gyre (Garcıa et al., 2002) and is associated with colder continental air masses (Reynolds and JM, 1981) and more extensive sea ice (Domack et al., 2003b; Ingólfsson et al., 2003; Michalchuk et al., 2009; Stammerjohn and Smith, 1996). The EAP is less influenced by westerly winds because of the peninsula (Bentley et al., 2009). In the Weddell Sea, the clockwise circulation of the Weddell Gyre brings warm CDW into the EAP (Orsi et al., 1990), turning the CDW into Weddell Sea Transitional Water (WSTW) (Barbara et al., 2016). During late winter, WSTW dominates Maxwell Bay within the SSI

(Yoon et al., 2010) on the WAP and slows the melting of local tide water glaciers. Thus, landmasses and surrounding bodies of water located at the northeastern tip of the peninsula might not be completely shielded or isolated from western influences due to low relief of the islands and oceanographic connections (Michalchuk et al., 2009).

2.2 Ongoing and past climate changes

Climate change in the AP region behaves differently than the continental interior of Antarctica. One such difference is how the two respond to Southern Annular Mode (SAM) events, associated with ENSO (Barbara et al., 2016; Kwok and Comiso, 2002; Stammerjohn et al., 2008). Positive SAM events correspond to warmer anomalies within the AP region and colder anomalies over the continent (Kwok and Comiso, 2002). Thus, a positive SAM event in the AP region is associated with reduced seasonal sea ice durations (Stammerjohn et al., 2008; Yuan, 2004) while the opposite holds true for negative SAM events. Additionally, Stammerjohn et al. (2008) suggests ice-atmosphere responses are strongest when a negative SAM event occurs with an El-Niño episode and when a positive SAM event occurs with a La-Niña episode. Furthermore, positive SAM events coupled with La-Niña episodes tend to strengthen northerly winds and cyclonic activity within the AP (Barbara et al., 2016).

In addition to the SAM, other climate forcing mechanisms drive climate change across the AP, such as greenhouse gases, solar insolation, ocean circulation changes, and the Southern Westerlies (Bentley et al., 2009). Forcing mechanisms can be enhanced because the narrow AP is geographically farther north than the continent and located within the Southern Westerly wind belt, which subjects the peninsula to strong marine and mid-latitude influences (Bentley et al., 2009).

Shifts in westerly winds and the Antarctic Circumpolar Current (ACC) are suggested to be the cause of rapid ice retreat in the WAP during the Holocene (Barbara et al., 2016;

Mulvaney et al., 2012; Shevenell et al., 2011). However, Barbara et al. (2016) suggests the EAP responded differently than the WAP because of the presence of the Weddell Gyre. Instead, the circulation of the gyre transported more fresh, cold surface waters, and sea ice northwards which slowed ice shelf retreat on the EAP and delayed seasonal open water conditions.

Over the Holocene, forcing mechanisms have produced shifts in climatic conditions, including the Early-Holocene climate optimum, Mid-Holocene warm period, Neoglacial interval, Mediaeval Warm Period, Little Ice Age, and the Recent Rapid Regional warming period. However, the various proxy records do not all record every one of these climate periods. The absence of climatic events might be caused by the analysis of different proxy records. For example, a marine core taken from the Palmer Deep, Site IODP 1098, records the Little Ice Age at around 700 to 150 yr (Domack et al., 2001; Domack et al., 2003b) while marine cores taken from the Firth of Tay and Maxwell Bay have no pronounced records of the Little Ice Age (Michalchuk et al., 2009; Milliken et al., 2009).

Bentley et al. (2009) described each of the Holocene climate periods. The Early Holocene Climate Optimum lasted from 11,000-9500 cal. ka BP. This period is characterized by significant widespread warming (Masson-Delmotte et al., 2004) and ice retreat across Antarctica during the early Holocene (Bentley et al., 2009; Domack, 2002; Domack et al., 2001; Evans et al., 2005; Pudsey et al., 1994). However, the Palmer Deep records colder conditions during this period. The contrasting records may reflect the importance of regional influences on the proxy records used in the studies. The timing of deglaciation seems to have started earlier on the WAP than the EAP (Bentley et al., 2009; Evans et al., 2005).

Deglaciation continued most likely at a slower rate during the period after the optimum from 9500-4500 cal. yr BP. During this time interval the WAP and EAP behaved differently (Bentley et al., 2009). Ice shelves on the WAP retreated and partially or completely reformed after the optimum (Bentley et al., 2005b; Smith et al., 2007) while ice shelves on the EAP remained intact (Domack et al., 2005). On a regional scale, some locations became ice free while others within the same area, including those within the same island chain, remained covered (Björck et al., 1996).

The Mid-Holocene Warm Period, also known as the Mid-Holocene Hypsithermal (MHH), was the next climate period of significant warming across the AP from 4500-2800 cal. yr BP. This period is associated with rapid sedimentation, high organic productivity, and increased species diversity in lake sediments (Björck et al., 1996; Björck et al., 1996; Hodgson and Convey, 2005; Hodgson et al., 2004) and reduced sea ice coverage, greater primary production, and increased sedimentation rates in marine sediments (Bentley et al., 2009; Domack et al., 2003b). However, unlike the optimum, not all proxy records across the AP indicate a significant warming trend during this period and the timing of the MHH varied by hundreds of years depending upon the proxy (Bentley et al., 2009).

A shift from warmer conditions to colder conditions marks the end of the MHH (Kulbe et al., 2001) and the start of the Neoglacial period. According to Bentley et al. (2009) the Neoglacial interval lasted from approximately 2500-1200 cal. yr BP and likely started earlier on the WAP (3600 cal. yr BP) (Domack, 2002) than the EAP (2500 cal. yr BP) (Bentley et al., 2009). Shevenell and Kennett (2002), suggest the earlier onset in the Palmer Deep was caused by an increase in cooler shelf waters and westerly winds. The climate conditions of this period are associated with more intense sea ice, cooler open water

conditions, a decline in biological productivity, and a glacial advance (Domack and Mcclennen, 1996). Recent work has constrained glacial advances to this time period (Kaplan et al., 2020; Palacios et al., 2020)

The Neoglacial period was followed by the Medieval Warm Period (MWP), which is thought to have lasted from 1200-600 cal. yr BP and is well documented in the Northern Hemisphere. However, it remains to be established in Antarctica because few proxies record evidence of the event. MWP evidence is restricted to few marine core records (Bentley et al., 2009) and a period of more restricted glacial ice around Palmer Station (Hall et al., 2010a; Yu et al., 2016). Similar to the MWP, evidence for the Little Ice Age (LIA) is fragmentary across the AP. The LIA is thought to have lasted from 700-150 cal. yr BP based on evidence from the Palmer Deep record (Shevenell and Kennett, 2002) and based on breaks in beach ridges on the SSI (Simms et al., 2012). Within the few locations in which it is found, the LIA is marked by a glacial advance, increased sea ice conditions, and colder sea surface temperatures (Bentley et al., 2009; Domack et al., 1995; Hall, 2009; Shevenell and Kennett, 2002). Further dating is required to determine if the timing of the glacial advances within the AP are coeval with the LIA in the Northern Hemisphere (Hall, 2009).

The warming period following the LIA is known as the Recent Rapid Regional (RRR) warming event and is marked by the pronounced warming trend that Antarctica is currently experiencing, most likely due to increased greenhouse gases in the atmosphere (Houghton, 2001). The RRR warming event is associated with increased sediment accumulation rates in a variety of proxy records such as lake and marine cores (Bentley et al., 2009), ice retreat, and reduced sea ice durations and snow cover (Vaughan et al., 2003).

2.3 Regional Sea Level Reconstructions

Glacial isostatic adjustment (GIA) plays an important role in controlling relative sea-level (RSL) changes in near-field settings. In the near-field, GIA results in uplift and falling sea surface heights due to reduced gravitational attraction between the ice and ocean following deglaciation, causing a RSL fall, while glaciation results in isostatic depression and more gravitational attraction between the ice and ocean, causing a RSL rise (Whitehouse, 2018). When coupled with GIA modeling, RSL reconstructions help constrain the size, extent, and timing of past ice sheets (Clark et al., 2002; Lambeck, 1993). One widely used recorder of RSL fall in Antarctica is raised beach ridges. RSL falls are preserved as beach ridges once the beach deposits are no longer influenced by wave exposure. However, tectonic uplift can also preserve beach ridges.

The SSI are located over an active subduction zone while the northern AP is a passive margin (Anderson, 1999; Nield et al., 2014). Therefore, active seismicity is centered around the SSI but less frequent along the rest of the AP (Kaminuma, 1995). Maximum estimates of long-term uplift rates for the SSI are on the order of 0.4-0.48 mm/yr (Watcham et al., 2011). These uplift rates are slower than the estimated ~2.8 mm/yr of Holocene GIA-induced uplift rates for the SSI (Fretwell et al., 2010) and an order of magnitude less than the estimated Holocene RSL change of 6.06 ± 4.72 mm/yr on Joinville Island (Zurbuchen and Simms, 2019). Although tectonics do play a minor role in uplift changes in the SSI, changes in beach ridge elevations largely reflect RSL changes from glacial isostatic rebound (Fretwell et al., 2010). Additionally, Zurbuchen and Simms (2019) suggest changes in Joinville's beach ridge elevations reflect isostatic rebound and not tectonic uplift.

Compared to other coastlines, relatively few studies of RSL changes are available for much of Antarctica due to limited ice-free locations. The few RSL records that do exist

across the AP are found within the SSI (Bentley et al., 2005a; Hall, 2010; Simkins et al., 2013; Watcham et al., 2011), Joinville Island (Zurbuchen and Simms, 2019), Marguerite Bay (Simkins et al., 2013), Torgersen Island (Simms et al., 2018), Alexander Island (Roberts et al., 2009), and Beak Island (Roberts et al., 2011). In the SSI, a sea-level high stand of 15.5 m on Fildes Peninsula occurred between 8000 and 7000 cal. yr BP years (calibrated years BP; present is defined as 1950 C.E.) (Watcham et al., 2011); thereafter, sea level is thought to have continuously fallen due to isostatic rebound. However, Hall (2010) suggests this fall may have been interrupted by transgressions at ~6000-7000 and 400 cal. yr BP, possibly in association with local glacial advances (Simms et al., 2012). On Joinville Island, Zurbuchen and Simms (2019) reconstructed a record of RSL based on the lower 18 of a flight of 31 beaches on the island. Radiocarbon ages from those lower 18 beach ridges reveal that RSL has fallen 4.9 ± 0.58 m over the past 3100 yr with an abrupt short-lived increase in the rate of RSL fall at 1540 ± 125 to 1320 ± 125 cal. yr B.P. and a potential RSL rise from 695 ± 190 to 235 ± 175 cal. yr B.P. (Zurbuchen and Simms, 2019).

2.4 Geochronology

The two most frequently used methods for dating raised beaches in Antarctica include radiocarbon dating and optically stimulated luminescence (OSL). The earliest attempts utilized radiocarbon dating of organic materials incorporated into the beach deposits (Baroni and Hall, 2004; Bentley et al., 2005a; Curl, 1980; Hall, 2010; Hall and Perry, 2004; Hansom, 1979; John and Sugden, 1971; Simkins et al., 2015). However, debate is ongoing on how to interpret the ages from the reworked materials. Remains from mobile species like birds or seals not limited to sea level usually provide a minimum age constraint for the beach (Simkins et al., 2015) while materials interbedded within the beach strata are assumed to be contemporaneous with beach formation (Hall, 2010) or reworked into the deposits thus

providing a maximum age for the beach (Bentley et al., 2005a). Alternatively, OSL dating has also been used to date beaches (Simms et al., 2011). Studies using OSL have argued that it more closely constrains the time of beach formation compared to radiocarbon dating as it dates the last exposure to sunlight (e.g. the last time the beach was active) (Hong et al., 2020; Simms et al., 2011). Studies from the South Shetland Islands (SSI) have shown that the ages derived from OSL are in broad agreement with previously published radiocarbon ages (Simms et al., 2012)

Raised beaches have been dated across the SSI but ages from the EAP are less common. Within the SSI, radiocarbon ages are particularly prevalent from beaches at elevations of 6 m, 10 m, 12 m, and 18 m (Birkenmajer, 1981; Birkenmajer, 1996, 1998; Fretwell et al., 2010; Hall, 2010; Hall, 2007; Hall and Perry, 2004; John and Sugden, 1971; Lindhorst and Schutter, 2014). However, slight variations in elevations of beach ridges of the same age are possible due to differences in wave exposure (Hall, 2010) and beach location with respect to the past ice mass center (Fretwell et al., 2010). Fretwell et al. (2010) surveyed the beaches within 15 locations across the SSI to constrain the pattern of regional isostatic uplift, in order to correlate beaches across the SSI. They identified three groups of beach ridges common among the islands at elevations between 4-6 m, 10-12 m, and 18-21 m. These groups of beach ridges date to 400-700 cal. yr BP for the 4-6 m beach ridges (Curl, 1980; Hall, 2010; Hall, 2003; Hall and Perry, 2004), 1800-2600 cal. yr BP for the 10-12 m beach ridges (Hall and Perry, 2004; Hansom, 1979), and around 7400-7500 cal. yr BP for the highest beach ridges usually located at the marine limit between 18 and 21 m (Hall, 2010; Hall, 2003).

Conversely, only one study has attempted to date the raised beaches on Joinville Island. Zurbuchen and Simms (2019) dated 17 raised beaches on Joinville Island ranging in age and elevation between 105 and 3095 cal. yr. BP and 0 – 11 m, respectively. The other well-constrained record of RSL along the EAP is a study of isolation basins on Beak Island. The transition from a marine to lacustrine environment was dated for three basins on Beak Island (Roberts et al., 2011). Roberts et. al (2011) found that for the highest basin with a sill at 11 m in elevation transitioned from marine to lacustrine conditions ~7200 cal. yr BP while basin 2 with a sill elevation of 2.4 m transitioned from marine to lacustrine conditions ~3000 cal. yr BP. Additionally, the sill within basin 3 is found at an elevation of 0.5 m and was isolated from the ocean ~1600 cal. yr BP. As no ages were obtained directly from the marine limit on the island, Roberts et al. (2011) estimated the age of the marine limit at ~15 m in two ways. An age of 8000 cal. yr BP was determined based on fitting a logarithmic curve to the other three index points while a linear extrapolation of relative sea level (RSL) change from basins 1 and 2 suggests an age of 8750 cal. yr BP. For this study, I assumed an age of 8000 cal. yr BP for the marine limit on Beak Island because it uses data from all three sills and RSL fall usually follows a logarithmic curve after deglaciation (Roberts et al., 2011).

2.5 Field Sites

2.5.1 Joinville Island

Tay Head Peninsula

Joinville Island is located at the northeastern tip of the Antarctic Peninsula between d'Urville Island and Dundee Island (*Figure 1*). These islands are a geological continuation of the Trinity Peninsula (Elliot, 1967). However, due to a combination of snow cover and sparse outcrops, little detailed mapping has been conducted on Joinville Island. A study by Elliot (1967) concluded that Joinville Island predominately consists of the Trinity Peninsula Series

and volcanic rock groups of the Andean Intrusive Suite of inferred Carboniferous to Tertiary age. Elliot (1967) mentions that although the Trinity Peninsula Series has not been studied in detail, it appears to mainly consists of folded clastic sedimentary rocks such as siltstones, sandstones, and conglomerates with their metamorphosed counterparts associated with later volcanic intrusions.

The 36 raised beaches observed on Joinville Island are approximately 400 m long and located on the east side of Tay Head, an approximately 2-2.5 km peninsula positioned on the south side of Joinville Island. The field site is adjacent to the Firth of Tay, 15 km from the location of a SHALDRIL core from which Michalchuk et. al (2009) obtained a high-resolution record of Holocene deglacial and climate history. The SHALDRIL core location experiences extensive sea ice cover, relatively cold Weddell Sea Transitional Water (Garcıa et al., 2002) and cold continental air masses (Minzoni et al., 2015) that result in an average annual temperature of -5°C (Michalchuk et al., 2009).

2.5.2 Livingston Island

South Beaches, Byers Peninsula

Livingston Island is approximately 160 km north of the AP located between Snow Island and Greenwich Island in the South Shetland Islands (SSI) (*Figure 1*). The west to east trending Byers Peninsula forms the western promontory of Livingston Island and is one of the largest ice-free areas in the SSI. Field observations indicate the predominate lithologies on Byers Peninsula are Tertiary basaltic agglomerates and augite-andesites (Hobbs, 1968) and fine-grained sedimentary rocks such as shales and sandstones (Lopez-Martinez et al., 1996). Regarding the raised Southern Beaches (62°40'S, 61°04'W) on Byers Peninsula, G. J. Hobbs (1968) describes the beach sediments as a derivative of the Younger Volcanic Group with occasional tonalite cobbles. The tonalite cobbles were likely derived from Barnard

Point, east of the South Beaches (Hobbs, 1968). The Younger Volcanic Group is Miocene in age and includes andesite and basalt lavas, tuffs, and agglomerates. However, the distribution of deposits across Livingston is not well known. Additionally, other features on the island include volcanic plugs, glacial deposits, raised marine platforms, caves, and tombolos that connect Vietor Rock and Stackpole Rocks to Livingston Island (Hobbs, 1968; Lopez-Martinez et al., 1996).

Byers Peninsula is frequented by periods of storminess, subjecting the area to strong north-westerly winds and a high-energy storm-wave environment. The strong winds drive large breakers toward the north-western coasts while the southern portion of the peninsula is more sheltered (John and Sugden, 1971). Subsequently, my site location is devoid of glacial ice and partially sheltered from the predominate northwest direction of most high-energy storm-waves (John and Sugden, 1971). Additionally, the South Beaches experience a maritime climate with average annual temperatures of -3°C (John and Sugden, 1971) and are located within the Southern Hemisphere storm belt (Davies, 1964). Subsequently, the westerly winds are linked with blowing snowfall off the island, which has been suggested as a contributing factor for the absence of a western extension of the Rotch Dome ice cap, which covers most of Livingston Island (Hobbs, 1968). However, the area receives more precipitation than the EAP.

3. Methods

Pebble roundness and grain-size were measured on 36 beaches while the prevalence of IRD was measured on 17 raised beaches on Joinville Island. Pebble roundness, grain-size, and prevalence of IRD were measured on 9 raised beaches on Livingston Island. All beaches were labeled starting at the closest proximity to the modern shoreline. Additionally, 58

cobble and sediment samples were collected on Livingston Island and 44 samples on Joinville Island for optically stimulated luminescence (OSL) age dating.

3.1 Granulometry

The size and roundness of the largest 100 surface clasts within a square meter area were observed, recorded, and photographed on 36 Joinville and 9 Livingston Island beaches for archival purposes similar to Simkins et al. (2015) and Bentley et. al (2005) (*Figure 2 and 3*). This process was repeated three times per raised beach. An additional 99 photographs were taken collectively along the length of each Livingston beach to bolster field roundness observations and characterize robust roundness trends. Clasts from the field and in photographs were classified into six categories: well rounded, rounded, sub rounded, sub angular, angular and very angular (Powers, 1953). Roundness data from a dip transect through the beaches was compared to the roundness data across the lateral length of beach 2 (the longest sampled beach) to determine if the variability between beaches is greater than the variability across a single beach (Hall, 2010). Grain size was measured according to the three longest axes of each pebble-cobble sized clast in the field on Livingston Island while Joinville clasts were measured according to the 2 longest axes observed in photographs. Standard deviation was used to describe sorting. Roundness and grain size measurements were not made in the field for clasts on Livingston's beach 3; however, these attributes were later measured in the office.

3.2 Ice Rafted Debris (IRD)

In the field, representative granule- to cobble-sized IRD clasts were sampled from each beach. Clasts not resembling local lithologies were considered to be IRD. The density of IRD clasts were measured along each beach to aid reconstruction of glacial activity and provenance. Calving glaciers produce icebergs capable of transporting and depositing IRD

onto beaches. However, the temperature and direction of the ocean current transporting the icebergs will determine where IRD is deposited. Cooler conditions enable icebergs to travel longer distances before melting (Matsumoto, 1996) and depositing IRD. Additionally, cooler climates are characteristic of sea ice. Therefore, open water conditions or limited sea ice should exist for icebergs to deposit IRD on the shoreline.

Hall and Perry (2004) considered all boulders located on Livingston Island beaches as IRD. Based on field observations some of the boulders were likely locally sourced from local outcrops or sea stacks in the modern or former surf zones (*Figure 4*). However, Byers Peninsula does not have a local source of granodiorite (Hall and Perry, 2004; Hobbs, 1968) with the closest tonalite rocks located at Barnard Point 40 km to the east. Therefore, on Livingston Island we only classified white porphyritic clasts >10 cm in diameter that contained quartz, plagioclase and biotite as IRD within a particular area on each beach. Trimble GPS coordinates plotted in ArcGIS provide an area measurement for determining IRD densities (cobble/m^2) for Livingston Island. On Joinville Island, 7 exotic lithologies were measured within 15 m^2 throughout the central portion of every other beach for IRD quantification.

3.3 Optically Stimulated Luminescence (OSL)

In order to determine beach ages, cobbles were sampled under lightproof conditions for optically stimulated luminescence (OSL) surface dating. An advantage of OSL is that it approximates the time elapsed since the last exposure of quartz and feldspar grains to sunlight with an age range up to 300-350 ka (Murray and Olley, 2002), six times the useful range of radiocarbon dating. Solar exposure resets crystals' natural signal by releasing electrons trapped in crystal defects (e.g. Si- or O- vacancies). The stimulated release of electrons is measured as the OSL signal. After solar exposure and subsequent burial of a

sample, irradiation from the surrounding materials causes electrons to reaccumulate within the crystal defects (Bøtter-Jensen, 1997; Simkins et al., 2016). Electron re-accumulation develops the natural signal, which increases the longer a sample is buried. Additionally, higher radiation doses produce larger trapped electron populations that create more intense OSL natural signals (Bøtter-Jensen and Murray, 2001), because the amount of trapped electrons is proportional to the radiation dose subjected to the sample. The radiation dose that the sample experienced during burial is estimated in the lab and is known as the equivalent dose. The dose rate, measured from surrounding materials, is also estimated. The division of the equivalent dose by the dose rate estimates OSL ages. However, grains used for dating must be sensitive to irradiation to produce a measurable signal. OSL sensitivity increases with more burial and exposure cycles proportional to the traveling distance (Singhvi et al., 2011). IRD clasts traveling longer distances than local rocks should accumulate a larger and more measurable signal for dating and are therefore targeted for sampling.

Dated cobbles provide a time series for beach changes, helping constrain wave climate conditions for both islands. We collected at least two samples for age validation per beach. Sample preparation and OSL dating methods follow Simkins et al. (2016). The top exposed portions are crushed for dose rate estimates. The unexposed or bottom portion of each sample was cut into ~2.5 cm plugs, limiting surface curvature, and without exposure to light. Subsequently, the outer 1 mm bottom cobble surface is removed following Simms et al. (2011), who demonstrated that the outer 1 mm surface was reset completely after one hour of daylight exposure. Any slice greater than 1.5 mm is thought to emit a non-representative luminescence signal and therefore was not used for dating. However, this process can be improved in future studies (Simkins et al., 2016). The target slices were crushed by hand

using a mortar and pestle in order to avoid pressures that could erase the luminescence signal. The carefully ground cobble sediment and sediment from sand samples were sieved for grain sizes 63-250 μ. The grains were then washed in 10% HCl and 27% H_2O_2 to remove carbonate and organic material contaminates. The remaining sediment from sand and cobble samples were density separated by 2.75, 2.62, 2.58, and 2.54 using lithium heteropolytungstate liquid (LST) to isolate quartz, potassium and sodium feldspars, heavy, and light grains. The heavy and light grains were saved and stored away while the remaining quartz and feldspar grains were etched using hydrofluoric acid. Using single aliquot regenerative (SAR) dose techniques (Murray and Wintle, 2000), these etched grains were placed into the Risø TL/OSL-DA-15 Reader manufactured by Risø National Laboratory for equivalent dose and dose rate measurements. Subsequently, ages of the samples were estimated.

3.4 GPS and Tide Gauge

Joinville Island GPS and tide data were collected in a previous campaign to Antarctica (Zurbuchen and Simms, 2019). Elevation and coordinate data were obtained using a UNAVCO Trimble Net R9 receiver global navigation satellite system (GNSS) base station and Trimble 5700 GPS/GNSS receiver. Upon failure of the local base station, the O'Higgins permanent GPS station (www.sonel.org), located ~115 km away from Joinville, was used instead. Beach-ridge profiles were obtained from kinematic mode GPS surveys across the crest of each beach ridge (*Figure 3*), except for beach ridges 2 and 3, which each have 3 static elevation points due to the presence of wildlife. GPS data was processed in Trimble Business Center with horizontal and vertical precisions of ~0.25 m. Elevations were converted to mean sea level using 2 days of data from a locally deployed Valeport 740

Portable Water Level Recorder (tide gauge) matched to the tide gauge at Bahia Esperanza ~50 km away.

Similar to Zurbuchen and Simms (2019), elevation and coordinate data were also collected using a UNAVCO Trimble Net R9 receiver and Trimble 5700 GPS/GNSS receiver on Livingston Island. All data were processed in Trimble Business Center relative to the WGS 1984 datum with horizontal and vertical precisions of <0.1 m. Beach profiles and IRD polygons were measured and recorded using kinematic-mode surveys while static points recorded the locations of OSL sample sites and roundness photographs. Beach crest heights are variable shore parallel; therefore, beach profiles provide a mean beach crest height for comparing beach elevations.

A Valeport 740 Portable Water Level Recorder (tide gauge) was installed 62° 39'45.7759" S, 61°0'42.8248" W to determine the tidal range for the study site. The gauge was calibrated to the salinity and temperature of the water at the time of deployment on February 24th, 2019. Pressure measurements were taken every five minutes for three days before kelp tore the transducer cord from the instrument box. The recorded pressure values were converted to depth measurements using the Valeport Terminal X2 software. Subsequently, the mean tide level (MTL) was measured by averaging the mean high water and mean low water marks from the three days of data.

As three days are not enough to determine a representative MTL, the closest available continuous tide data set obtained from Palmer Station, Antarctica was used as an analogue site. The estimated 20-year National Tidal Datum Epoch (NTDE) for Palmer Station was used to correct the Livingston tide data following the NOAA Computational Techniques for Tidal Datums Handbook standard method for mixed tides (Evans et al., 2003). The corrected

MTL for Livingston Island is 0.790 m relative to our tide gauge sensor. This MTL was used as a baseline to adjust the Trimble GPS elevations to approximate local MSL.

3.5 Age Compilation

Beach ridge ages on Joinville and Livingston Islands were estimated using previously published radiocarbon ages (*Table 1 and 2*). Zurbuchen and Simms (2019) obtained radiocarbon ages for the lower 21 beach deposits (labeled 0-18 including 7a, 7b, 15a, 15b) on Joinville Island, except for beach ridge 14 (*Figure 3*). The ages range from 105 $\pm$ 160 (beach 1) to 3095 $\pm$ 195 cal. yr BP (beach 18). Based on these radiocarbon ages, the average rate of beach formation is approximately every 176 years. An extrapolation of that rate for the upper 15 raised beaches provides an estimated age for beach 31 of about 5800 cal. yr BP. Additionally, the elevation of Joinville's youngest beach ridge 1 was subtracted from the elevations of the other 30 beaches to provide an estimate of past relative sea levels above (modern) mean sea level (amsl) following the methodology of Fretwell et al. (2010).

In order to determine if the beach ridge age estimates are reasonable, I compared the estimated beach ridge age amsl elevations to isolation basins from Beak Island (Roberts et al., 2011) less than 200 km away. The proximity of Joinville and Beak Island implies the changes in RSL between islands should be similar. Subsequently, the estimated ages produce a best fit line slope similar to the Beak Island isolation basin RSL record (*Figure 5*).

On Livingston Island, 17 radiocarbon ages were compiled from previous studies conducted in the SSI (*Figure 6*). Two ages were taken from Hansom (1979) at the prevalent elevation of 10 m equivalent to our beach ridge 4; five ages from Hall and Perry (2004) at prevalent elevations of 6 m and 10 m equivalent to our beach ridges 2 and 4; and ten ages were taken from Hall (2010) at the prevalent elevations of 6 m, 12 m, and 18 m equivalent to our beach ridges 2, 5, and 9 (*Figure 7*). The Hall and Perry (2004) ages were obtained from

beach ridges contiguous with those in this study but located about 1 km to the west of our field site. Each radiocarbon age was converted to calendar years using CALIB 7.1 (Stuiver and Reimer, 1993; Stuiver et al., 1998) with the MARINE 13 dataset (Reimer et al., 2013) and a delta-*R* value of 791 $\pm$ 121 (Hall et al., 2010b), derived from Antarctic corals. However, strand plain deposits identified in this study have not been dated using radiocarbon. Subsequently, strand plain ages are estimated using the average rate of beach formation based on the distance between beach ridges.

5. Results

5.1 Joinville

5.1.1 Beach Characteristics

Based on 9,092 grain size measurements, the pebbles within Joinville Island's 36 beaches on average range between 2-4 cm in maximum length with an overall standard deviation of 1.11 cm (*Figure 8A*). Fine grains (e.g. diameters <2 mm) were almost absent within the upper 15-cm of the beach deposits (*Figure 9*). Additionally, the mean grain size and sorting of pebbles on Joinville Island beaches do not change more than 1 cm through time (*Figure 8*). However, the sedimentary characteristics differed between the upper and lower beach deposits. The deposits of the lower 21 beaches were stratified with mats of seaweed within their matrix while the deposits of the upper 15 beaches were not stratified and lacked seaweed.

Roundness measurements performed on 4,025 pebbles indicate the lower Joinville beaches are more rounded than the upper beaches (*Figure 8b*). Coarser grains are more easily rounded than finer grain sizes (Boggs, 1995), which could bias the roundness trends. However, after performing a form of hypothesis test on the data, the results failed to reject the null hypothesis of no correlation (see *Appendix A, Figure A3*). Therefore, grain size does

not have an effect on grain roundness. Of the 36 beach deposits, 9 modes are well-rounded; 24 modes are rounded; 2 modes are sub-rounded; and 1 mode is sub-angular (*Figure 8B*). The general increase in roundness through time is interrupted at beaches 5, 13-15.5, and 28 (*Figure 8b*). Beach 5 exhibits less and beach 28 exhibits more rounding than the general trend (*Figure 8b*). The transition from beaches 15.5 through 13 indicates a decrease in roundness over time, opposite the overall roundness trend.

The less rounded deposits of beach 5 also have the most IRD of any Joinville Island beach while a slight increase in IRD is seen throughout the transition from beaches 15.5 to 13 (*Figure 10*). Unfortunately, IRD data was not directly collected for beach 28.

5.1.2 Age Model

Radiocarbon ages for the lower Joinville beaches were produced from shell and seaweed materials interbedded within the beach deposits and range from 105 $\pm$ 160 (beach 1) to 3095 $\pm$ 195 cal. yr BP (beach 18) (*Figure 3*). Assuming an average rate of beach formation of 176 years, the ages for the upper beach deposits range from 3347 (beach 19) to 5800 cal. yr BP (beach 31). Best fit lines of age vs elevation (amsl) for Joinville and Beak Islands have slopes of 2.1 mm/yr and 2.2 mm/yr, respectively (*Figure 5*). Joinville Island beach ridges were on average 2.23 m higher than time equivalent RSLs on Beak Island. However, the marine limit of ~15 m amsl on Beak Island is estimated to be 8000-8750 cal. yr BP while Joinville Island's marine limit is ~11 m amsl with an estimated age of ~5800 cal. yr BP. On Joinville Island the beaches (including the highest) are cut into 2, possibly 3, moraines; therefore, older beaches could have been eroded or prevented from forming due to the presence of glacial ice. Unfortunately, the GPS data for Joinville Island beach ridges 22 and 23 is unreliable. Therefore, those ages are not included in figure 5, which creates an artificial break between ~6.5 - 8.5 m amsl.

5.2 Livingston

5.2.1 Beach Characteristics

The South Beaches on Byers Peninsula are approximately 10 km long. I focused my field observations on the central portion of the beaches southwest of Negro Hill (*Figure 2*). We identified nine beaches within the study area of which five were beach ridges and three were part of the strand plain. The beach ridges rise higher above the surrounding topography than the strand plain beaches (*Figure 11)*. Beach 1, the modern beach, is a combination of a strand plain and beach ridge deposit (Lindhorst and Schutter, 2014) while beaches 2, 4, 5, 8 and 9 are beach ridges and beaches 3, 6 and 7 are part of the strand plain. Beaches 8 and 9 were located at the base of a cliff and next to a paleo-sea stack, respectively. Those local sources may have biased roundness and grain size measurements from beaches 8 and 9 (*Figure 2*). Both the beach ridges and strand plains on Livingston Island contain poorly sorted stratified sand and gravels with ample quantities of fine-grained materials (e.g. diameters <2 mm) and very little organic material (e.g. only a handful of bones were observed) (*Figure 12*). A few bones were observed on the surface of the beaches and thus their relationship with the timing of beach formation was unknown and they were not sampled for radiocarbon analysis.

Grain size measurements were performed on 2,600 surface clasts pebble sized (0.63 cm) or larger while roundness measurements were performed on 39,456 clasts. The roundness mode for Livingston Island beach deposits is sub-rounded while the maximum length of surface clasts on average ranges from 2-6 cm with an overall standard deviation of 1.57 cm (*Figure 13*). Additionally, no coherent trends in grain size with respect to time were observed on the beaches of Livingston Island, which may be a function of the limited time series (*Figure 13)*.

The beach ridges and strand plain deposits differed in their grain size and roundness. Beach ridge deposits are coarser and more poorly sorted than the strand plain deposits (*Figure 13a*). The proximity of beach 8 to Negro Hill likely contributed to the largest standard deviation (2.71) in grain size values measured on the island. The strand plain deposits contained more sub-angular to sub-rounded sediments while beach ridge deposits contained more sub-rounded to rounded deposits (*Figure 13b*).

With the exception of field measurements on beach 8, more variability in roundness was observed between beaches within a dip transect ($\sigma = 0.16$) than along the length of a single beach ($\sigma < 0.10$) (e.g., beach 2 in *Figure 14*). However, after performing a form of hypothesis test on the data, the results failed to reject the null hypothesis of no correlation (see *Appendix A, Figure A3*). Therefore, grain size does not have an effect on grain roundness. Beach ridges have higher IRD densities than the strand plains (*Figure 15*). The most IRD is found on beach ridges 2 and 4, supporting the findings of Hall and Perry (2004), while beach 3, a strand plain, had no visible IRD. Additionally, beaches 4 and 5 have similar sedimentary characteristics but have sharp contrasts in IRD counts with beach 4 having a higher IRD density (*Figure 15*).

5.2.2 Age Model

Radiocarbon ages were compiled and recalibrated from previous studies (*Figure 7*) (Hall, 2010; Hall and Perry, 2004; Hansom, 1979). The radiocarbon sample elevations were used to match our beaches to the prominently sampled beach ridges across the SSI using the isobars of Fretwell et al. (2010). Additionally, the relative IRD densities collected in this study appear to correlate with those of the neighboring study of Hall and Perry (2004), which supports our beach age assignments (*Table 2*). Most of the ages were obtained on whalebones on Livingston Island's South Beaches with the exception of ages on beach 5.

Beach 5 correlates to the 12 m beach on Greenwich Island, which was dated using buried seaweed (Hall, 2010) (*Figure 1*). The assigned ages for each beach ridge are listed in cal. yr BP with a 2σ error (*Table 2A*) while strand plain ages are estimated using the average rate of beach formation between beach ridges based on lateral distance (*Table 2B*).

6. Discussion

6.1 Island Comparison

Wave exposure and energy are important factors in the formation of beaches (Hall, 2010; Simkins et al., 2015). Livingston Island is positioned in a maritime climate zone, while Joinville Island lies within the colder Weddell Sea and experiences continental winds (Michalchuk et al., 2009). The colder climate of the EAP favors the development of extensive sea ice coverage (Barbara et al., 2016; Stammerjohn and Smith, 1996). Sea ice prevents wave exposure to the shoreline, inhibits storms from reworking beach deposits (Simkins et al., 2015) and prevents icebergs from depositing IRD (Hall and Perry, 2004). Limited wave exposure also impedes beach formation and clast rounding. Google Earth images and aerial photographs compiled by the logistics division of United States Antarctic Program indicate sea ice is more prevalent during the winter season; however, sea ice can form or remain during the summer months as well (e.g. image from December 2009 in *Figure 16*). With its location within the Weddell Sea and on the EAP, Joinville experiences more prevalent sea ice conditions, inhibiting beach processes for larger portions of the year. Conversely, the warmer climate of the WAP is not as favorable for the development of sea ice.

The differences between the overall average grain size and standard deviation recorded on Livingston and Joinville Islands are 0.31 cm and 0.46 cm, respectively (Table 3 and 4). After performing hypotheses tests on the data, the high p-value of 0.2886 indicates

that I cannot reject the null hypothesis that the average grain sizes are from populations with equal means (see *Appendix A, Figure A4*). However, the low p-value of 0.0086 indicates that I can reject the null hypothesis that the variances in standard deviations are equal between islands (see *Appendix A, Figure A5*). Thus, Livingston beach deposits are more poorly sorted than Joinville beach deposits. Furthermore, only the largest surface clasts were measured on Livingston because the beaches contained prevalent fine-grained sediments (mostly sand) too small to measure in the field. Thus, the difference in standard deviation is a minimum difference. Additionally, had I taken into account the sand sized material, the hypothesis test may have resulted in a significant difference in mean grain size between the two islands. On Joinville Island, no sand or finer grained material was observed in the upper 15 cm of the beaches. Typically, fine-grained deposits within a high energy environment are removed by swash processes when subjected to long durations of open water (Forbes et al., 1995). Livingston beaches are exposed to wave action nearly year-round, suggesting the presence of fine grains on Livingston Island is not caused by limited wave exposure due to sea ice, nor has consistent high energy wave action removed the finer grains from the beach deposits. Alternatively, Joinville Island is subjected to large amounts of seasonal sea ice that would be expected to hinder wave exposure. The lack of sand on Joinville Island beaches implies consistent high wave energy and low sediment supply has resulted in the removal of finer grains from the beaches (Forbes et al., 1995). On the other hand, limited wave exposure conflicts with the observed more rounded Joinville Island beach deposits compared to those of Livingston Island.

The shoreface profile of Livingston is shallower (0.008) than the profile at Joinville (0.017). The shallower shoreface slope of Livingston likely leads to the attenuation of waves

before crashing onto the shoreline, whereas steep gravel beaches are often associated with high wave energy and sediment deficiency (Butler, 1999). Wave attenuation could explain the finer grained deposition along Livingston beaches. Additionally, Livingston has strand plain deposits, which are indicative of normal swash conditions. Larger waves could attenuate along the shallow shoreface so much so that they act as normal swash processes upon reaching the shoreline. Furthermore, Livingston Island contains creeks that flow from the upper 35 m platforms towards the ocean, features not present on Joinville Island. These creeks may provide sand and other fine sediment to the beaches of Livingston Island. Therefore, I suggest the lack of fine grains on Joinville Island is caused by a combination of consistent high energy waves and a sediment deficiency to the beaches. Additionally, the higher wave energy causes Joinville beach deposits to be more rounded compared to Livingston. The harder rocks of Joinville Island (metasedimentary and metamorphic (Elliot, 1967)) compared to the rocks of Livingston Island (volcanics and fine-grained sedimentary rocks (Lopez-Martinez et al., 1996)) may also contribute to the differences.

6.2 Joinville Beach Roundness

Beaches 5, 13-15.5, and 28 interrupt the overall roundness trend on Joinville Island (*Figure 8b*). These interruptions do not correlate with inferred RSL changes described by Zurbuchen and Simms (2019), which suggests these differences were caused by factors other than changes in the rate of RSL. Beach 5 contains less rounded materials and formed 1045 $\pm$ 135 cal. yr BP. A tentative correlation is made between a negative SAM event and the formation of beach 5, which indicates that climate conditions were cooler during the formation of beach 5 as the Southern Westerlies likely shifted towards the equator (Kaplan et al., 2020; Kwok and Comiso, 2002; Moreno et al., 2018) (*Figure 17*). The temperature anomaly record from the James Ross Island ice core (Mulvaney et al., 2012) supports this

suggestion as temperatures were low at the time and continued to decrease thereafter (*Figure 17*). Additionally, anomalously low roundness measurements are also found in Marguerite Bay (Simkins et al., 2015) during the formation of Joinville Island beach 5. Thus, the reduced rounding of sediments within beach 5 could be the result of less open water conditions with an increase in sea ice observed in the relative abundance of diatom assemblages (Barbara et al., 2016), indicative of cooler temperatures (*Figure 17*). Additionally, beach 5 has the highest IRD count, which further supports the importance of cooler temperatures during the formation of beach ridge 5. Cooler temperatures might have led to a glacial advance on Joinville Island and surrounding regions and supplied more icebergs carrying IRD (Bond et al., 1992). According to Mulvaney et al. (2012), a permanent ice shelf formed after ~1500 cal. yr BP within the Prince Gustav Channel, which offers a potential source of IRD for beach 5. Additionally, ice advances on James Ross Island (Björck et al., 1996) and nearby islands (Balco and Schaefer, 2013) occurred at or after 1400 cal. yr BP.

A large break-out of icebergs can also be caused by warming temperatures. The formation of beach 5 is tentatively correlated to the end of a negative SAM event and the beginning of the Medieval Warm Period (MWP). The MWP occurred from 600 to 1200 cal. yr BP with evidence of Antarctic warming seemingly restricted to the WAP and found mostly in marine records (Bentley et al., 2009), such as the Palmer Deep Site 1098 (Domack et al., 2003b). Terrestrial organic material on Anvers Island also records reduced ice from 700-970 cal. yr BP (Hall et al., 2010a). Additionally, other studies along the WAP record evidence for warmer conditions (Guglielmin et al., 2016; Hall, 2007; Khim et al., 2002) but warm events seem to be more strongly expressed on the WAP than the EAP (Bentley et al., 2009). Although the high IRD count for Joinville's beach 5 could have been caused by

retreating glaciers during warmer conditions, evidence for the MWP was not documented in the SHALDRIL marine core taken in the Firth of Tay, 15 km from Joinville (Michalchuk et al., 2009). Therefore, I am more inclined to suggest the high IRD density on beach 5 was deposited under colder climate conditions.

The next interruption in Joinville's roundness measurements is the transition from beach 15.5 to 13. This transition exhibits a potential increase in IRD with a decreasing pebble roundness, which could reflect an introduction of more angular material. The ages of beaches 15.5-13 (~2800-2300 cal. yr BP) correspond to the onset of the well documented Neoglacial time period ~2500 cal. yr BP (Bentley et al., 2009). Pronounced cooling on James Ross Island supports the onset of the Neoglacial period at 2500 cal. yr BP (Mulvaney et al., 2012). However, evidence from a SHALDRIL core taken in the Firth of Tay on the EAP suggests the Neoglacial period lasted from 3500 cal. yr BP to present (Michalchuk et al., 2009) similar to findings on the WAP in the Palmer Deep Site 1098 (Domack, 2002; Shevenell and Kennett, 2002). Joinville Island has relatively low relief and might not be as shielded from western climatic influences as regions farther to the south. Therefore, the timing of the onset of the Neoglacial interval for Joinville Island might be better represented by ~3000 cal. yr BP.

Additional proxy evidence across the AP supports cooler climate conditions around 3000 cal. yr BP (*Figure 17*). Therefore, the prolonged cooling associated with the Neoglacial time period could explain the increase in IRD and increasing sea ice conditions associated with the Neoglacial interval could have hindered clast rounding, causing the decrease in roundness trend, but not enough to prevent icebergs from landing on the shore.

Finally, beach 28 had more rounded beach materials compared to the overall roundness trend (*Figure 8b*). Using an estimated age of ~4900 cal. yr BP from the average rate of beach progradation, beach 28 potentially formed during a period of increased open water and decreased sea ice conditions (*Figure 17*). These conditions are suggested by the warmer conditions in the proxy record of relative abundance of *T. Antarctica T2* and diatom assemblages (Barbara et al., 2016). The increased wave exposure from prolonged open waters may have resulted in a higher percentage of rounded clasts within beach 28.

6.3 Joinville Glacial Advance

Two readily identifiable local lithologies were observed while counting IRD on Joinville Island: a low-silica rhyolite and sandstone/quartzite. Beaches 0-21 contained more low-silica rhyolite clasts while beaches 27-31 contained less rhyolite and more sandstone clasts (*Figure 18)*. The decrease in sandstone occurred between beaches 21 and 27. This decrease could be a manifestation of a change in sources. Outcrops of the sandstone are located west of the three present ground moraines while the low-silica rhyolite was present as dikes within low grade metamorphosed fine-grained sedimentary rocks in the sea stacks and outcrops on the eastern side of Tay Head (*Figure 3*). The rocks within the westernmost moraine behind beach ridge 31 were dominantly sandstone. Therefore, the sediment source for the upper beaches was most likely the moraine and sandstone outcrops to the east, and as beaches became preserved eventually, the sandstone sources were abandoned or swamped by materials from other parts of the peninsula. Subsequently, the dominant sediment source transitioned to the low grade metamorphosed fine-grained sedimentary rocks with the low-silica rhyolite dykes for the lower beaches. However, this transition does not align with changes in pebble roundness, indicating processes other than just a source change caused the

changes in roundness. Although, the age of the westernmost moraine is unknown, beach 31 cuts into the moraine suggesting it is likely older than 5800 cal. yr BP.

Two other ground moraines are present north of the beaches on Tay Head Peninsula (*Figure 3*). Although, the sandstone would have been transported east by glacial ice to form the upper moraine and hence sourced the upper beaches, the low-silica rhyolite and its affiliated low grade metamorphosed fine-grained sedimentary rocks are readily present in the area. The easternmost two moraines appeared to be composed of these rocks. The middle of the two moraines cuts across beaches 21-24 and thus postdates 3700-4200 cal. yr BP while the lower moraine cuts across beach 12 and thus post-dates 2240 $\pm$ 155 cal. yr BP.

6.4 Livingston Beach Ridge Roundness vs Strand Plain Roundness

The beach ridge deposits on Livingston Island contain more poorly sorted materials with higher percentages of rounded clasts than strand plain deposits on the island. I suggest the beach ridges were deposited during storm events because Livingston Island is located within the Southern Hemisphere storm belt (Davies, 1964). Additionally, the small number of preserved beach ridges on the South Beaches are suggestive of discrete periods of storminess. Storms strongly influence beach deposits by eroding newly formed beaches and leaving behind a singular large deposit (Butler, 1999; Scheffers et al., 2012). Additionally, storm deposits are typically coarser (Scheffers et al., 2012), more angular, and poorly sorted (Butler, 1999). Conversely, strand plains are deposited by swash sedimentation under calm conditions (Lindhorst and Schutter, 2014) and are typically finer-grained and better sorted (Dominguez et al., 2009; Forrest, 2007). Therefore, I expected the beach-ridge deposits to be more angular compared to the strand plains, but we see the opposite relationship (*Figure 13*). Lower IRD frequencies indicate warmer conditions during strand plain formation, suggesting greater sea ice is not a factor for the differences in clast roundness. Furthermore, ground

penetrated radar profiles through the beach ridges image overwash deposits (Gernant et al., 2020). Overwash deposits occur when water and sediment flows over a beach crest during storms. Subsequently, storms capable of producing overwash deposits can erode beaches within the storm wave limit and bury older strand plain deposits. Therefore, we suggest the heightened roundness of Livingston Island beach ridge deposits is due to the recycling of older strand plain deposits. As the deposits are recycled during a storm, the materials are further rounded, causing the beach ridges to have larger and more rounded beach deposits than the strand plains.

6.5 Do these two locations record similar climatic changes?

The paleoclimate indicators preserved within the sedimentary deposits of raised beaches on Joinville and Livingston Islands provide an opportunity to compare similar proxy records from the western and eastern sides of the Antarctic Peninsula. The granulometry trends and IRD densities from the two islands appear to be out-of-phase during some time periods (~1100 cal. yr BP) and in-phase during other time periods (~1800 cal. yr BP) over the last ~3,000 years. Joinville Island beaches 15.5-13 (2800-2300 cal. yr BP) formed during the well-documented Neoglacial period (~3000 cal. yr BP) and are marked by a resetting of the roundness trend while no beaches of similar age have been dated or described on Livingston Island (Hall, 2010; Hall, 2009). In addition to this notable absence of pronounced beaches within the SSI from a time period of notable beach development on Joinville Island, the sedimentary characteristics of other time equivalent beaches on the two islands reflect notable differences, which may reflect differences in regional climate drivers. For example, the largest and least rounded beach pebbles and the highest IRD density on Joinville Island are found on beach 5, which formed around 1045 $\pm$ 135 cal. yr BP (*Figure 17*). Conversely, Livingston Island's beach 3, which formed around the same time, ~1130 cal. yr BP, is

characterized by the smallest and least rounded beach pebbles and no IRD (*Figure 13 and 15*). The most rounded pebbles and the highest IRD occurrences on Livingston Island are found on beach ridges 2 and 4, which formed at 420 ± 474 and 1840 ± 611 cal. yr BP, respectively. On Joinville Island, the time-equivalent beach ridge 2 of Livingston Island has been removed by erosion from 695 ± 190 to 235 ± 175 cal. yr BP (Zurbuchen and Simms, 2019) while no remarkable sedimentary characteristics were observed for Joinville beach ridge 11, which formed at 1888 ± 150, the time-equivalent beach of Livingston beach ridge 4. Overall, for the climatic shifts at ~1100 and ~1800 cal. yr BP, the sedimentary characteristics thought to reflect climatic conditions on the two island's beaches appear to be out-of-phase.

Extensive sea ice forms during cold conditions on the EAP (Domack et al., 2003a; Ingólfsson et al., 2003; Stammerjohn and Smith, 1996), which limits wave action on beaches (Butler, 1999), while sea ice is not as extensive on the WAP. For example, the EAP is characterized as having permanent ice fields and multiyear sea ice while the WAP is characterized by seasonal sea ice (Stammerjohn and Smith, 1996). The relative abundance (%) of the Sea Ice Assemblage, interpreted as a proxy for sea ice duration (Barbara et al., 2016) on the EAP, indicates the duration of sea ice is increasing during the formation of Joinville Island's beach 5 (1045 ± 135 cal. yr BP) and peaks during the Joinville Island hiatus in beach formation (695 ± 190 to 235 ± 175 cal. yr BP) (Figure 17). Although sea-ice was not extensive enough to prevent the formation of beach 5, it was extensive enough to limit the rounding of its beach materials. Additionally, the duration of sea ice is seemingly higher during the Joinville Island hiatus in beach formation than during the formation of

beaches 3 and 2 that mark the beginning and end of the hiatus, respectively. Thus, the increase in duration of sea ice offers a potential explanation for the hiatus.

Based on erosion, Zurbuchen and Simms (2019) suggest the hiatus in beach formation resulted from a rise in RSL driven by GIA-driven uplift. As suggested by Zurbuchen and Simms (2019), the hiatus corresponds to cooler temperatures across the Antarctic Peninsula (Ahmed et al., 2013) and glacial advances on both sides of the peninsula (Davies et al., 2014; Domack et al., 1995; Kaplan et al., 2020). The hiatus also corresponds to the timing of the LIA on the WAP (Domack et al., 2003b). However, evidence from the James Ross Island ice core and Beak Island lake sediments indicate a warming event began ~600 cal. yr BP (Mulvaney et al., 2012; Sterken et al., 2012). Kaplan et al. (2020) suggests glaciers within the northern AP and around James Ross Island were larger than normal from ~2400-1000 cal. yr BP and from ~300-100 cal. yr BP. Additionally, Davies et al. (2014) suggests the James Ross Island ice core displays a temperature-precipitation dependence of 0%. Therefore, glacial advances during the Joinville Island hiatus likely drove isostatic depression within the region causing a RSL rise. Subsequently, the transgression associated with the cold period was likely the driver of beach erosion during the hiatus. Thus, comparisons of sedimentary characteristics to other time-equivalent beaches cannot be made because they were eroded.

An erosional surface is also located under Livingston Island's beach 2 which formed 420 ± 474 cal. yr BP, similar in time to the hiatus in beach ridge formation on Joinville Island. Ground penetrating radar images overwash deposits at the crest of Livingston's beach 2 (Gernant et al., 2020) which indicates periods of storm activity predominantly influenced the beach deposit, producing more rounded beach pebbles. Additionally, Hall (2009, 2010)

suggests this time period corresponds to a RSL rise potentially linked to glacial advance in the SSI. Therefore, the climate drivers that formed Livingston's beach 2 and the Joinville hiatus seem to be in-phase around 400 cal. yr BP. However, direct comparisons cannot be made between Livingston's beach 2 and the Joinville hiatus because the sedimentary characteristics were eroded on Joinville.

Livingston Island's beach 3 formed during the MWP observed on the WAP from 1150-700 cal. yr BP) (Domack et al., 2003b), while no evidence for the MWP was recorded in the Firth of Tay sediment core record in the EAP adjacent to Joinville Island (Michalchuk et al., 2009). Instead, cold conditions were observed on the EAP during Joinville Island's time-equivalent beach 5, for Livingston Island's beach 3. However, Michalchuk et al. (2009) indicates more detailed analyses could reveal evidence for smaller-scale events such as the MWP and LIA within the Firth of Tay record. In turn, Joinville Island could have experienced a warming period. However, no time-equivalent beaches exist for Joinville Island's beach 5 on Livingston Island, which supports the idea that the beaches are out-of-phase approximately 1100 cal. yr BP.

The dichotomy in climate between the EAP and WAP reflected in the granulometry and IRD record at ~1100 and ~1800 cal. yr BP is similar to that seen within some records of glacier expansion (*Figure 19*). Glacial advances on the EAP were recorded on James Ross Island and nearby islands ~1500 cal. yr BP (Balco and Schaefer, 2013; Björck et al., 1996; Kaplan et al., 2020). Additionally, ice shelves reformed on the EAP around 1500 cal. yr BP (Brachfeld et al., 2003; Pudsey et al., 2006). However, terrestrial peat records from Anvers Island on the WAP record a warm period during the time period from 2300-1200 cal. yr BP (Yu et al., 2016). The cold period from 900-600 cal. yr BP on the WAP (Yu et al., 2016) is

more suggestive of a Little Ice Age-like glacial advance and is similar in timing to the formation of Livingston Island's beach 2 at 420 ± 474 cal. yr BP, which has the second highest IRD density on Livingston Island. This suggests cold periods like the one beginning ~1500 cal. yr BP occur on the EAP prior to the WAP. However, more data are needed to confirm this climatic dichotomy as a few records appear to contradict the timing of some of these events. For example, a warm period on Anvers Island was recorded in terrestrial organic material records 970-700 cal. yr BP (Hall et al., 2010a), a time period suggested by Yu et al. (2016) to be marked by cold conditions (*Figure 19*).

7. Conclusion

In order to reconstruct past environmental conditions along the northeastern and western Antarctic Peninsula, I documented the changes in grain-size, roundness of grains, and ice-rafted debris frequency of 36 raised beaches on Joinville Island and nine raised beaches on Livingston Island. The beach ridges on Joinville Island extend back to 5800 cal. yr BP while those on Livingston Island date back to 7500 cal. yr BP. No coherent trends in grain size were observed on the beaches of Livingston Island while the beaches on Joinville Island grain size shows low variability in grain size. The beach deposits on Livingston were more poorly sorted than those on Joinville Island. The difference between the sorting of the beaches from the two islands likely reflects the steeper foreshore gradient on Joinville Island (0.017) compared to Livingston Island (0.008).

On Joinville Island, roundness generally decreases with age with the exception of beaches 5, 15.5-13, and 28. Upon comparing the interruptions to proxy data across the AP, beach 5, which dates to 1045 ± 135 cal. yr BP and contains less rounded clasts, likely formed during a period of cooler climate conditions. Prolonged cooling associated with the

Neoglacial period may have hindered clast rounding during the formation of the more poorly rounded beaches 15.5-13, deposited between 2800 and 2300 cal. yr BP. The anomalously high percentage of rounded materials in beach 28, which formed around 4900 cal. yr BP, may reflect a period of longer open water conditions and minimal to no sea ice.

A transition from more sandstone clasts to low-silica rhyolite clasts occurs between upper beach ridges 21-27, ~3700-4800 cal. yr BP. This transition does not coincide with a disruption in the decrease in roundness with age. Instead, the transition in clast lithology reflects a source shift from sandstones within the moraine located at the landward limit of the raised beaches to the more locally sourced rhyolite and fine-grained metasedimentary rocks found in outcrops and paleo-sea stacks of the beaches.

Variations in the characteristics of Livingston Island beaches largely reflect the differences between strand plain and beach ridge deposits. The beach ridge deposits are coarser and more poorly sorted than the strand plain deposits. The sub-angular to sub-rounded strand plains are thought to be deposited during calm conditions while the sub-rounded to rounded beach ridge deposits are typically interpreted to have been deposited during storm events. Despite the coarser and more poorly sorted sediments of the beach ridges, their roundness exceeds that of the strand plain deposits. As ground penetrating radar profiles through the beach ridges suggest the presence of strand plain deposits beneath the beach ridges, the increased roundness of the overwash deposits on the beach ridge may reflect the eroded and recycled nature of their deposits.

Livingston Island is subjected to the warmer ACC and Southern Westerly wind belt, which overall decreases sea ice extent and duration on the WAP while Joinville Island on the EAP is subjected to colder waters and more extensive sea ice from the Weddell Gyre. This

climatic dichotomy is reflected in my granulometry and IRD record as time-equivalent beaches on Joinville and Livingston Islands display contrasting sedimentary characteristics (e.g. Joinville beach 5 [1045 $\pm$ 135 cal. yr BP] has the largest average grain size and highest IRD frequency while Livingston beach 3 [1130 cal. yr BP] has the smallest average grain size and no IRD).

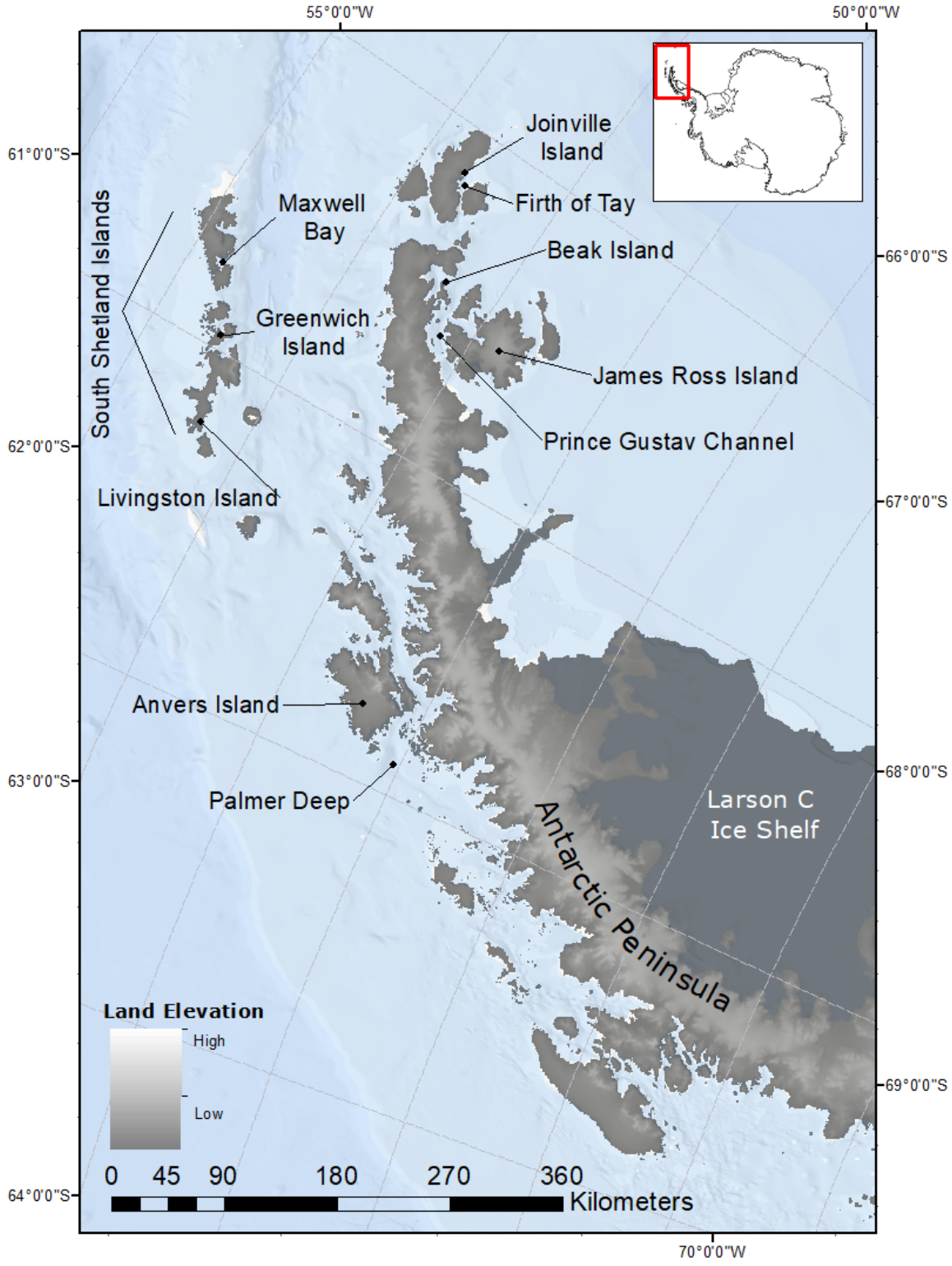

Figure 1: Map illustrating field sites and Antarctic Peninsula locations.

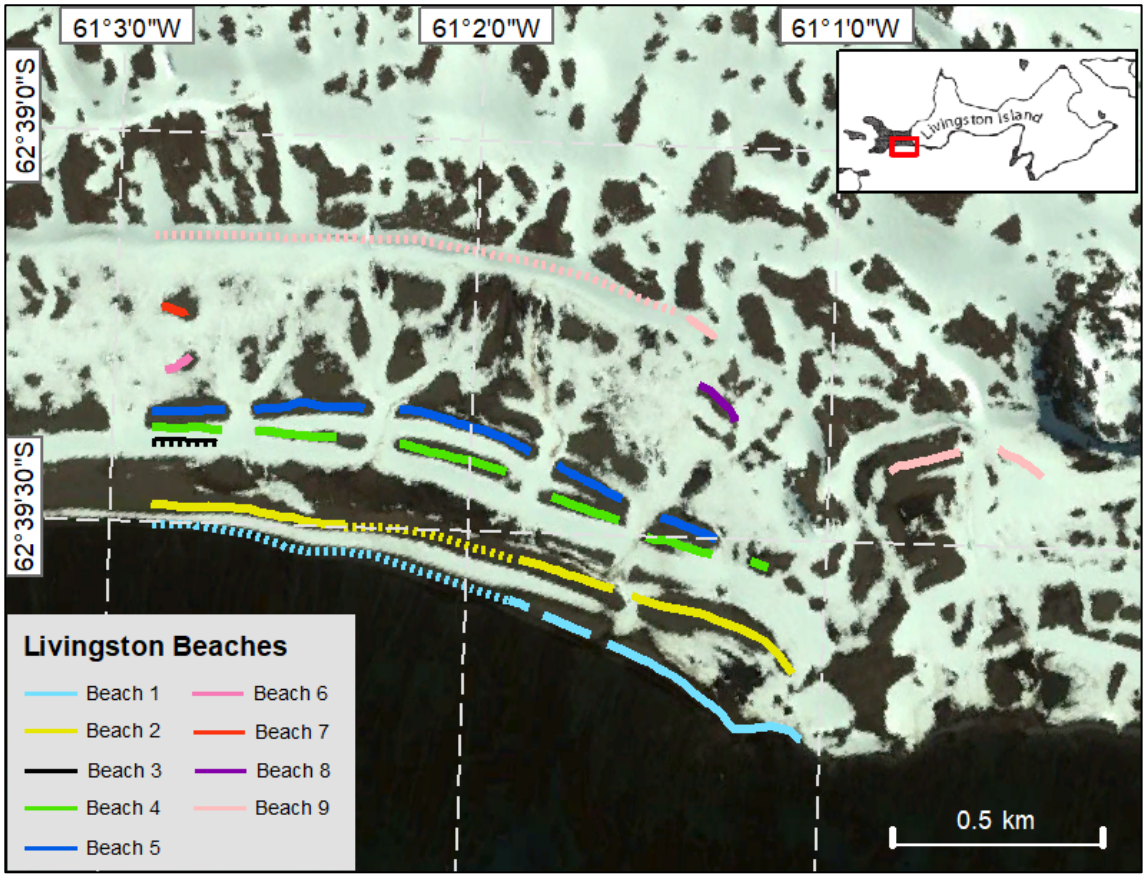

Figure 2: Map of Livingston Island beaches. Solid lines indicate where kinematic GPS surveys were taken and dotted lines indicate projected locations.

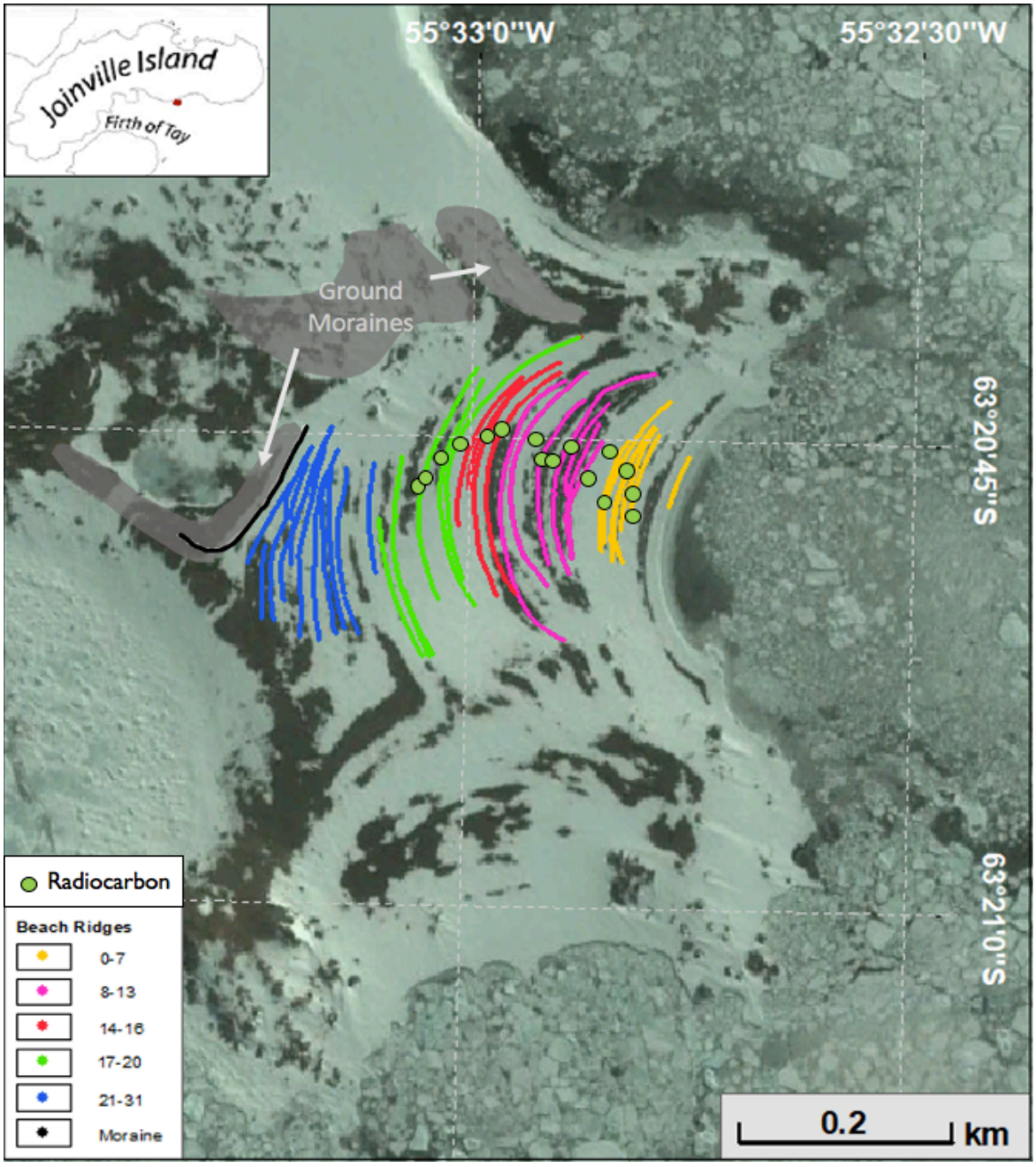

Figure 3: Map of Joinville Island beaches. Beaches 22 and 23 are not displayed because GPS data could not be processed. Black line is a measured moraine that sits at the marine limit. The relationships between the three different ground moraines are unclear.

Figure 4: Image of sea stacks, indicated by arrows, on South Beaches of Livingston Island viewing east from the modern beach.

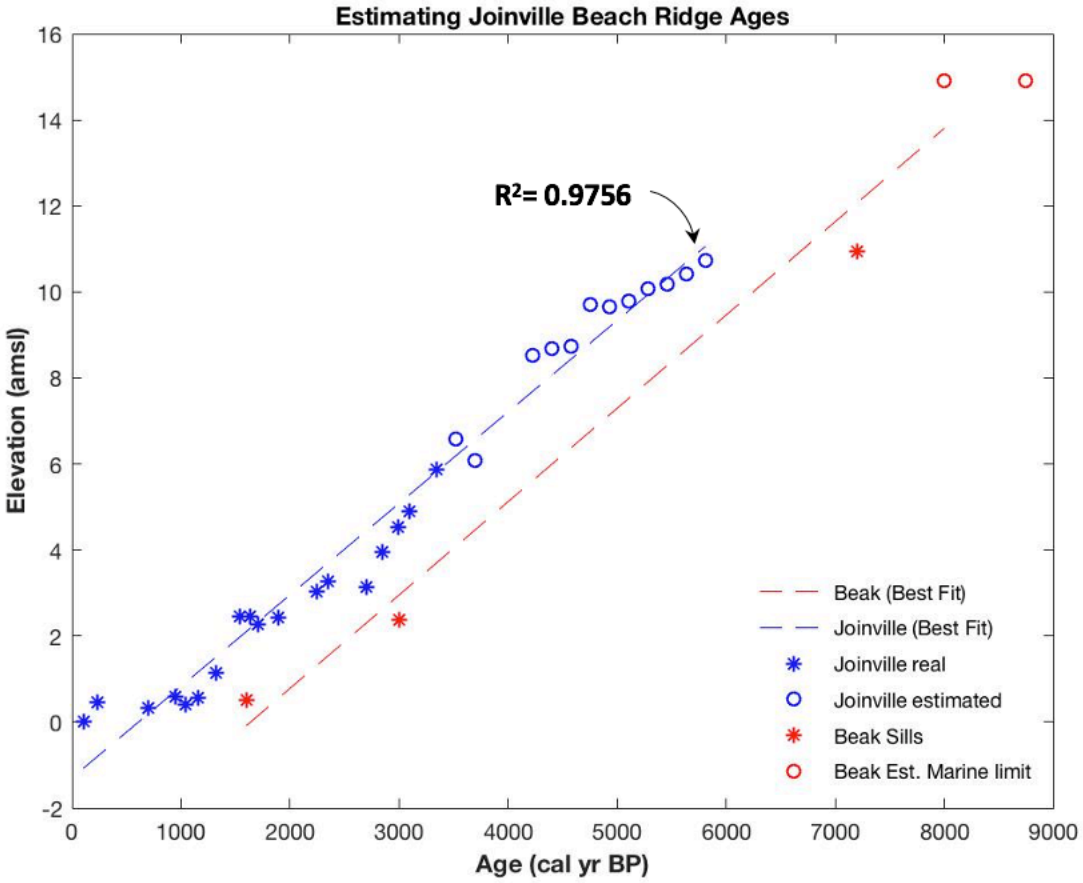

Figure 5: Joinville Island beach ridge estimated ages vs Beak Island basins. Best fit line slopes of Joinville and Beak Island are 0.0021 and 0.0022, respectively. Beach ridges 22 and 23 are not included because elevation data does not exist. In turn, there is a gap between 6.5-8.5 m amsl.

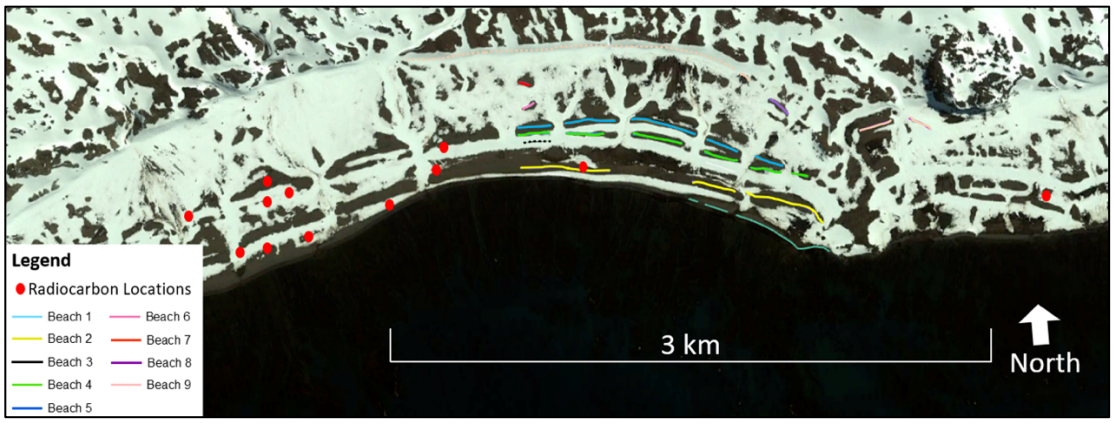

Figure 6: Previous radiocarbon sampling locations from Livingston Island. Radiocarbon ages used for beach 5 were taken from Greenwich Island (not pictured). Additionally, definitive locations could not be made for the two Hansom (1979) sample sites and the age for beach 9 was estimated in Hall (2010).

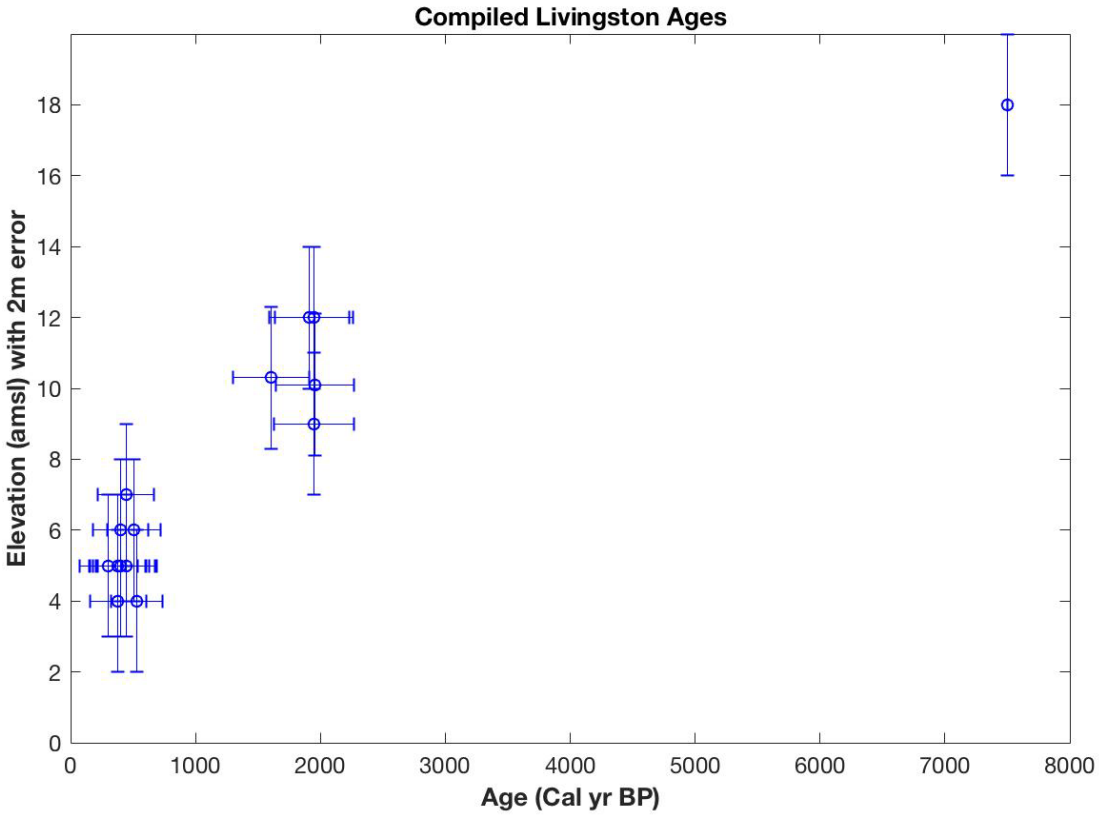

Figure 7: Seventeen compiled radiocarbon dates for Livingston Island. The 18 m beach does not have horizontal error bars because age was an estimation from Hall (2010). Vertical error of 2 m was given because waves exposure can cause as much as 2 m variability in beach height within the same sample site (Hall, 2010).

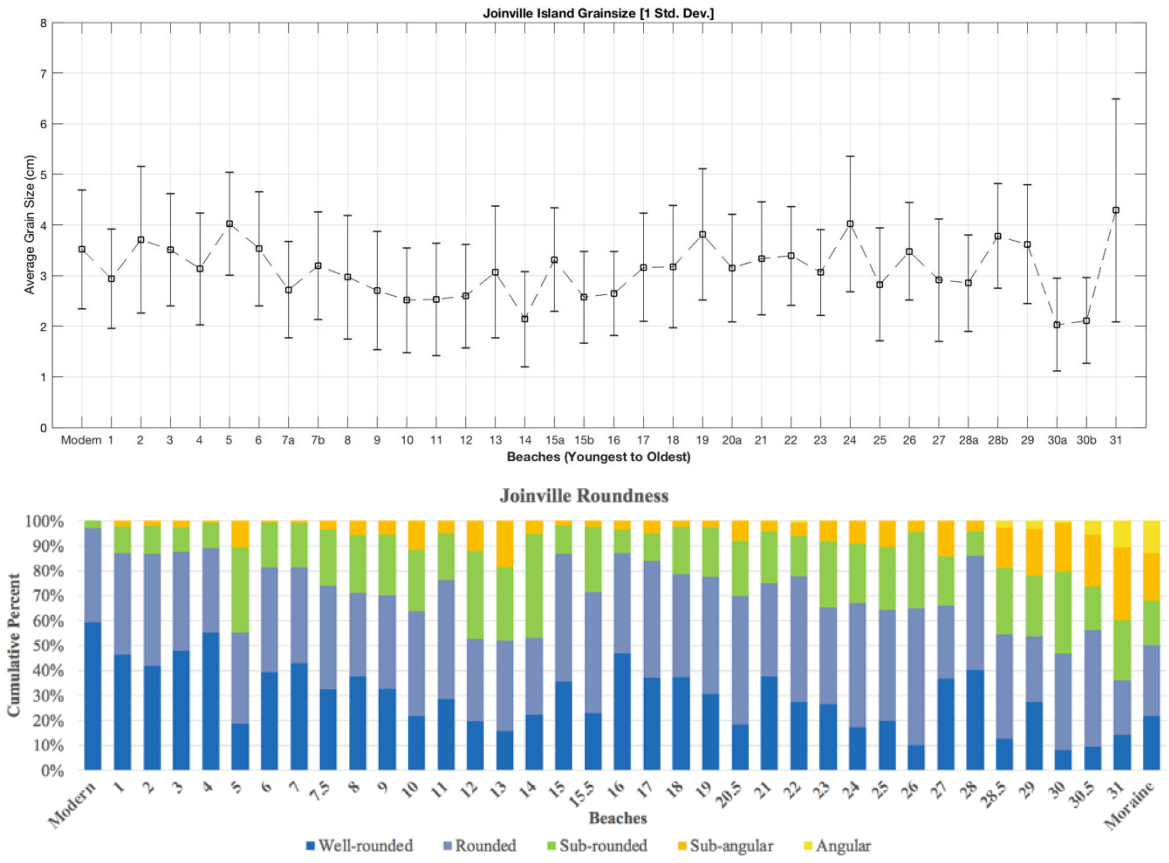

Figure 8: Top) Average a-axis grain size measurements and **Bottom)** Average roundness and mode of all Joinville Island beaches

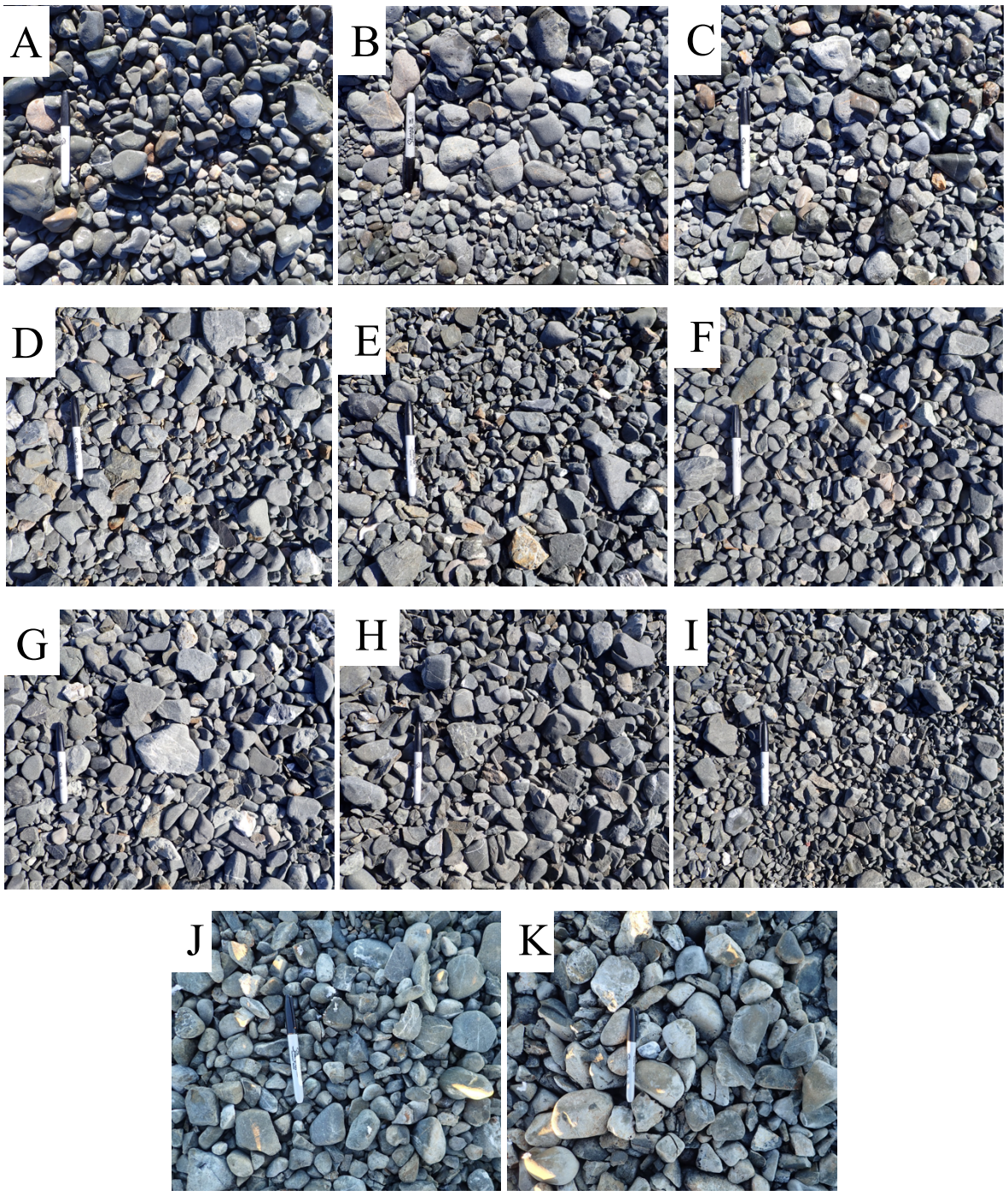

Figure 9: Images of Joinville Island beach materials for the A) modern beach, B) beach 3, C) beach 6, D) beach 9, E) beach 12, F) beach 15, G) beach 18, H) beach 21, I) beach 25, J) beach 28, and K) beach 31.

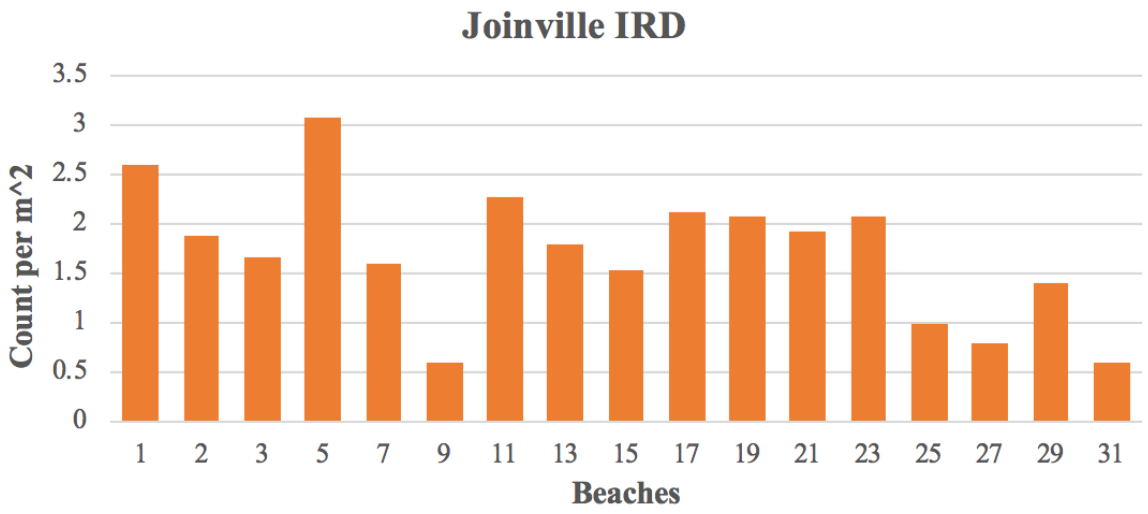

Figure 10: IRD densities for Joinville Island. The IRD counts were collected within 15 m^2 along the central portion of every other beach.

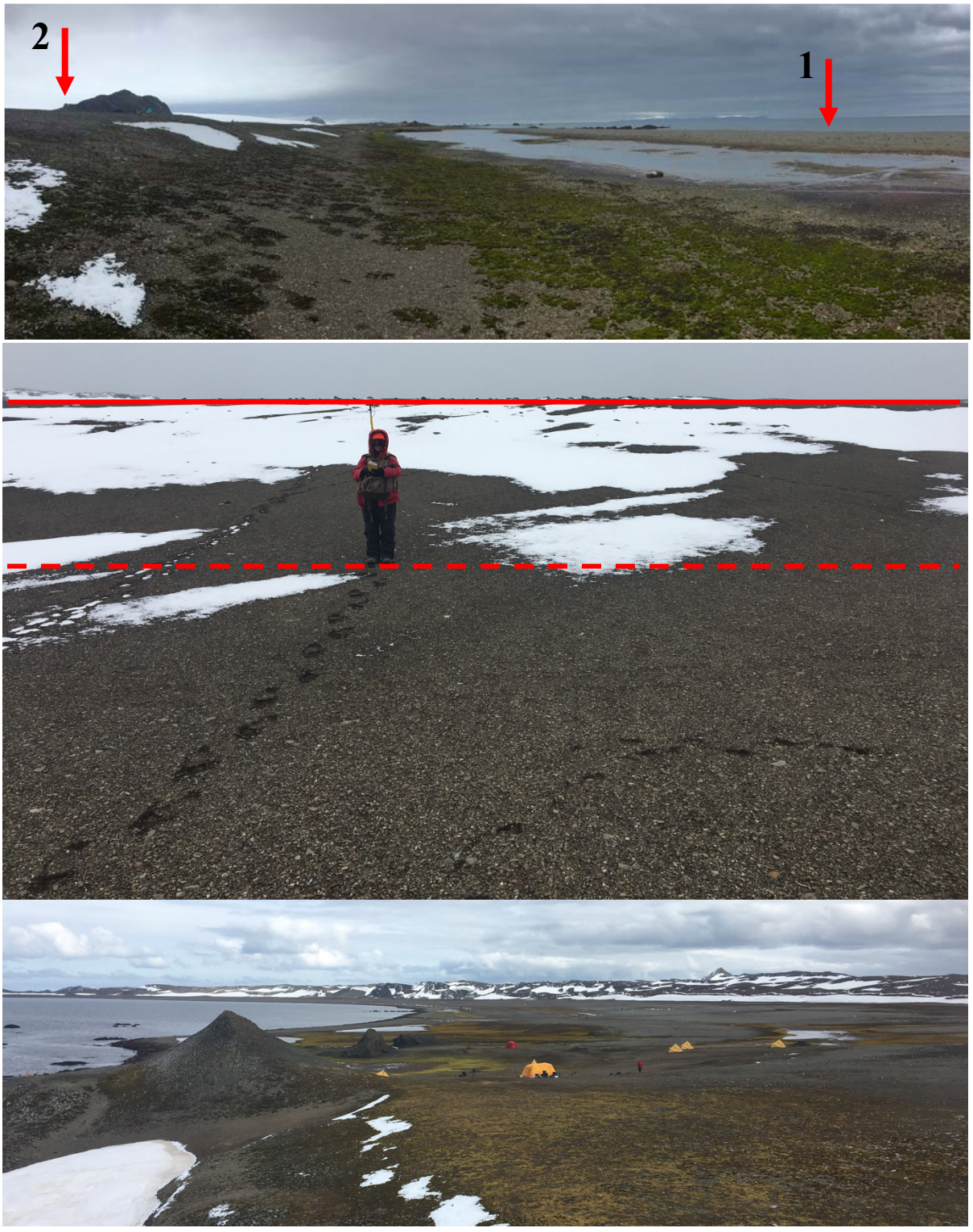

Figure 11: Landscape images of Livingston Island beaches. Top image views beaches 1 and 2 looking west, middle image depicts topography change from beach 3 (dashed line) to beach 4 (solid line), and the bottom image views east, looking at all the beaches.

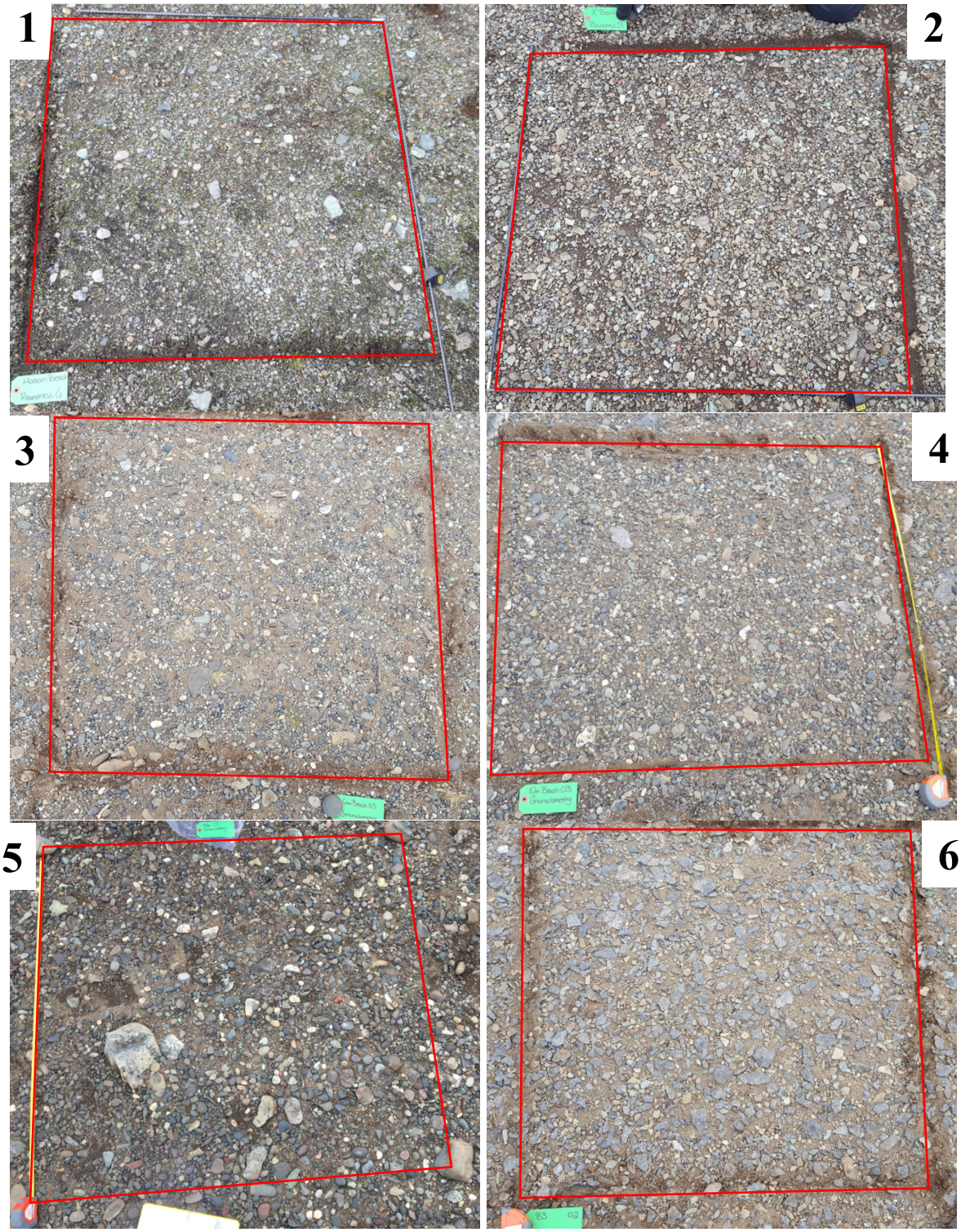
1
2
3
4
5
6

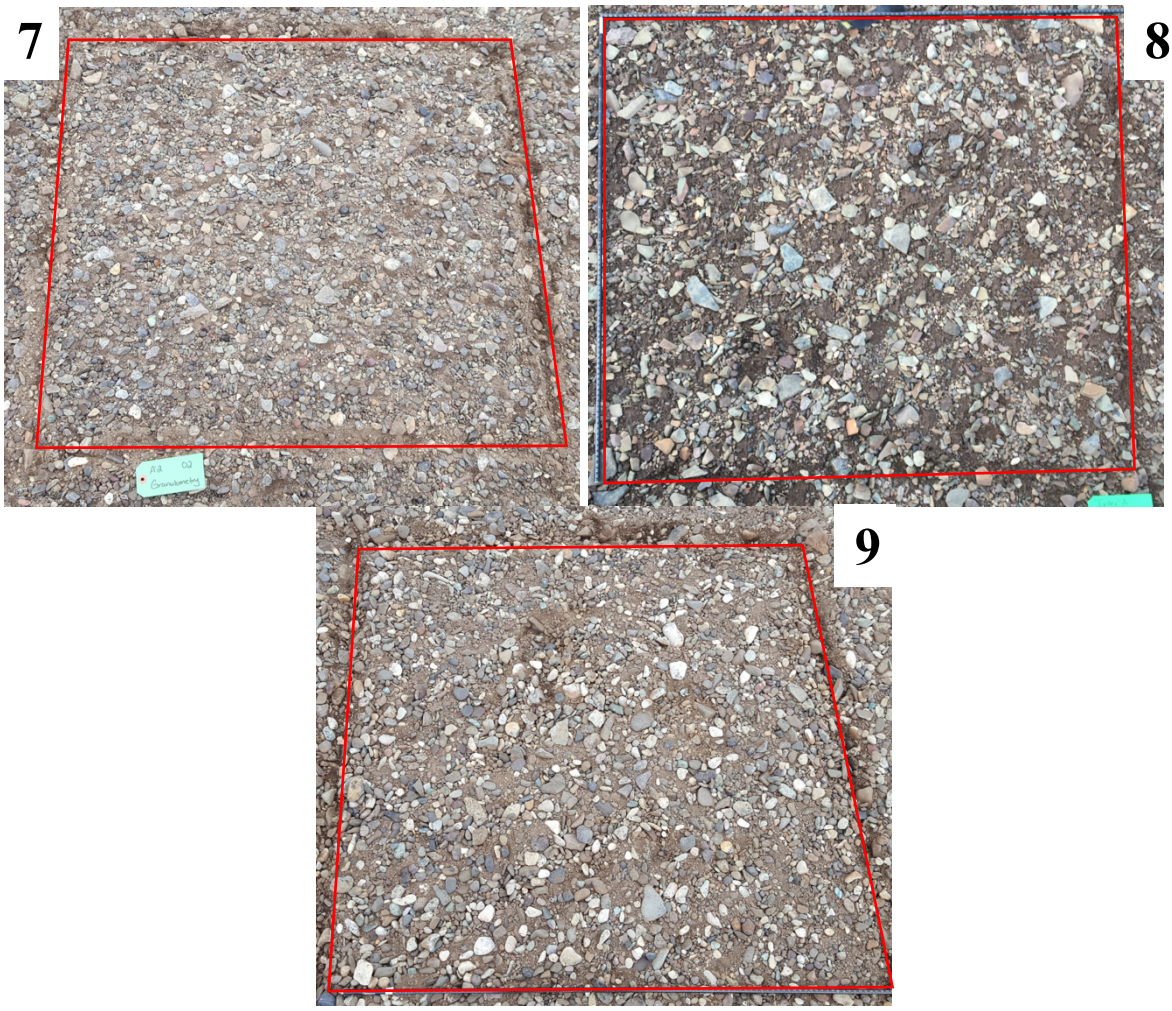

Figure 12: Images of beach materials for Livingston beaches 1, 2, 3, 4, 5, 6, 7, 8, and 9.

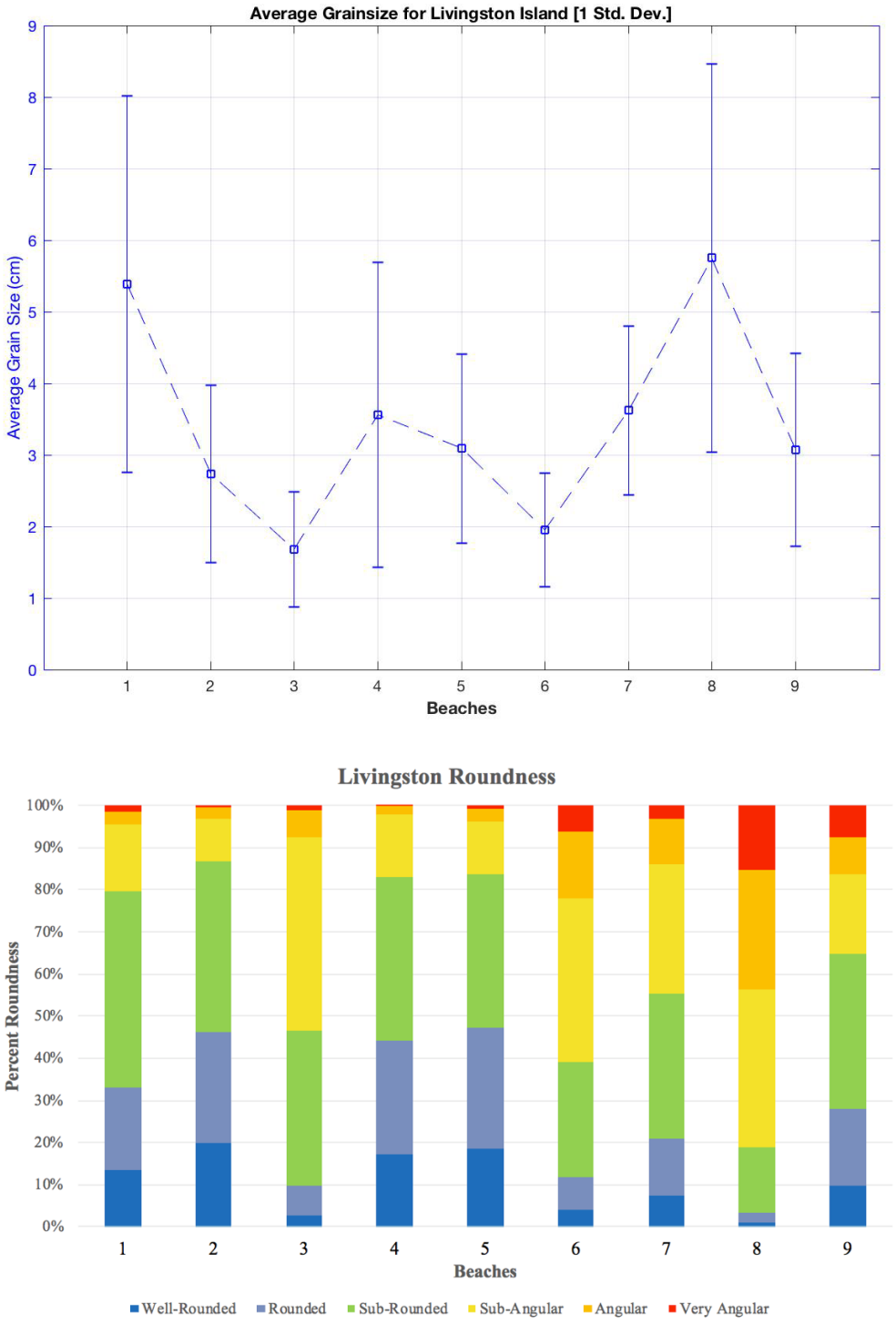

Figure 13: **Top)** Average a-axis grain size measurements. **Bottom)** Cumulative roundness measurements for Livingston beaches.

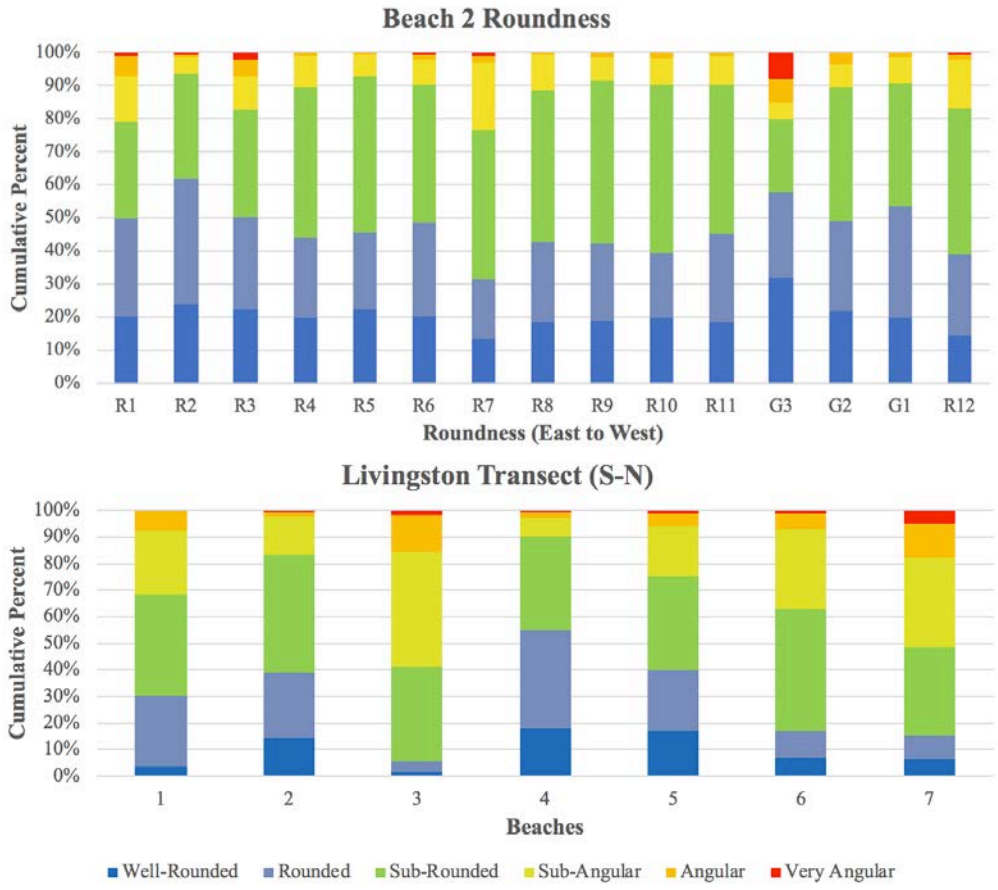

Figure 14: Top) East to West roundness measurements along the sampled length of beach 2, standard deviation of 0.05. **Bottom)** Roundness measurements along South to North transect, standard deviation of 0.16.

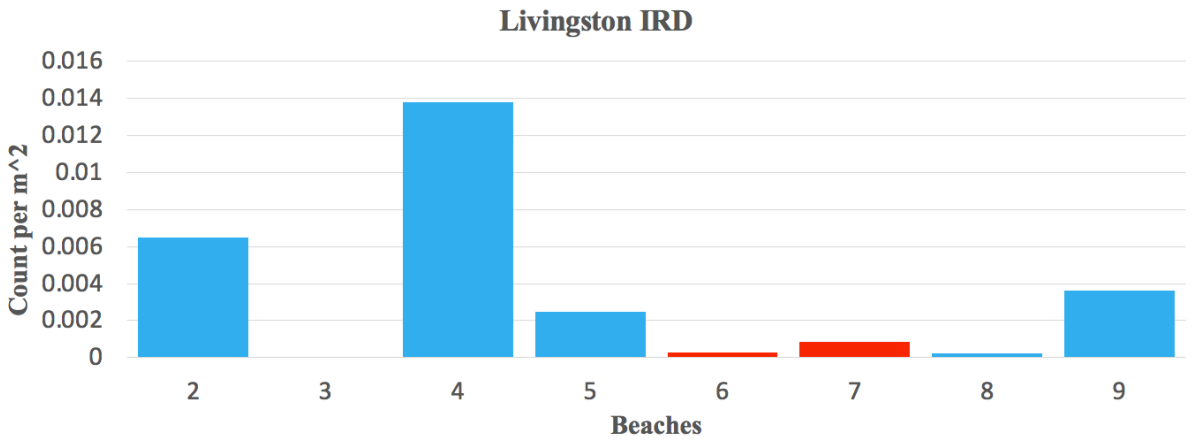

Figure 15: IRD densities for Livingston Island (beach ridges in blue and strand plains in red). White medium-grained clasts containing quartz, plagioclase, and biotite with diameters >10cm were considered IRD. Measurements were made within specific locations along the beach.

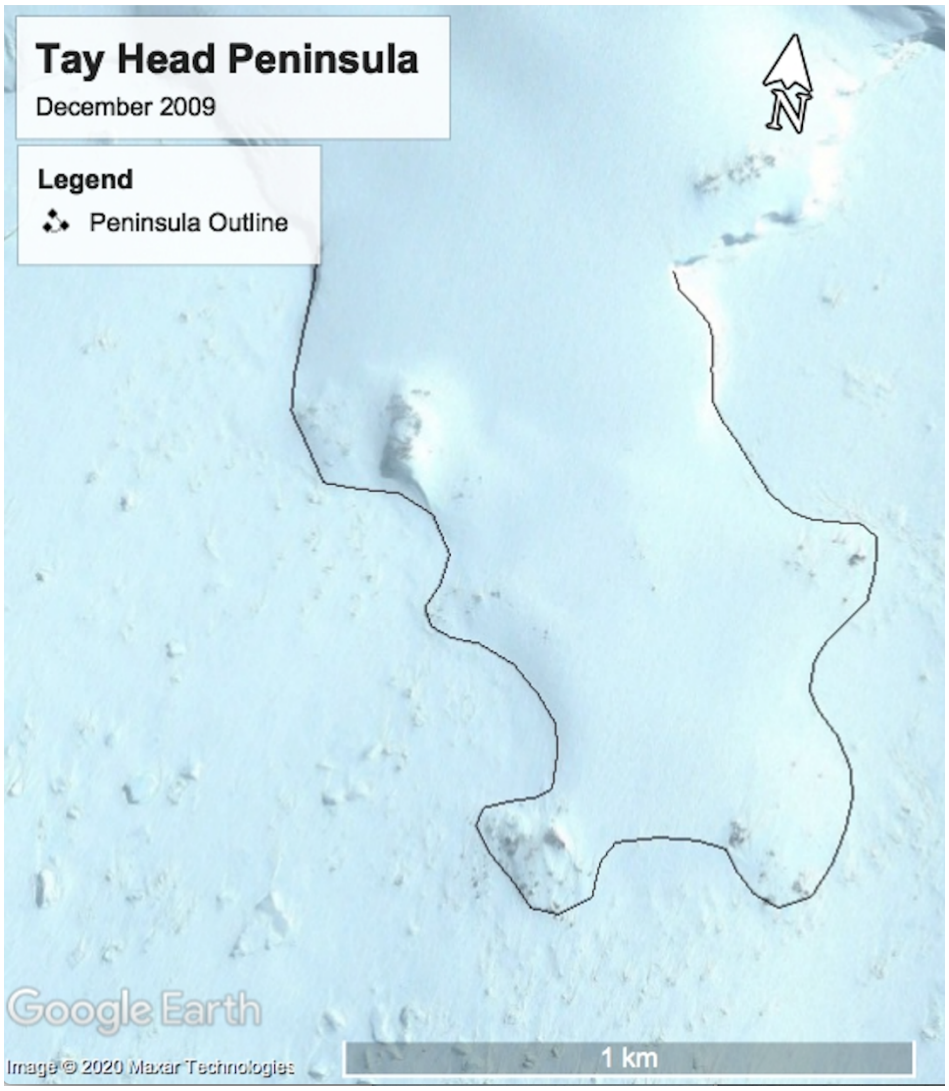

Figure 16: Google Earth Image from December 2009 of Tay Head Peninsula. Sea ice and snow cover can surround the peninsula during the summer months, such as December.

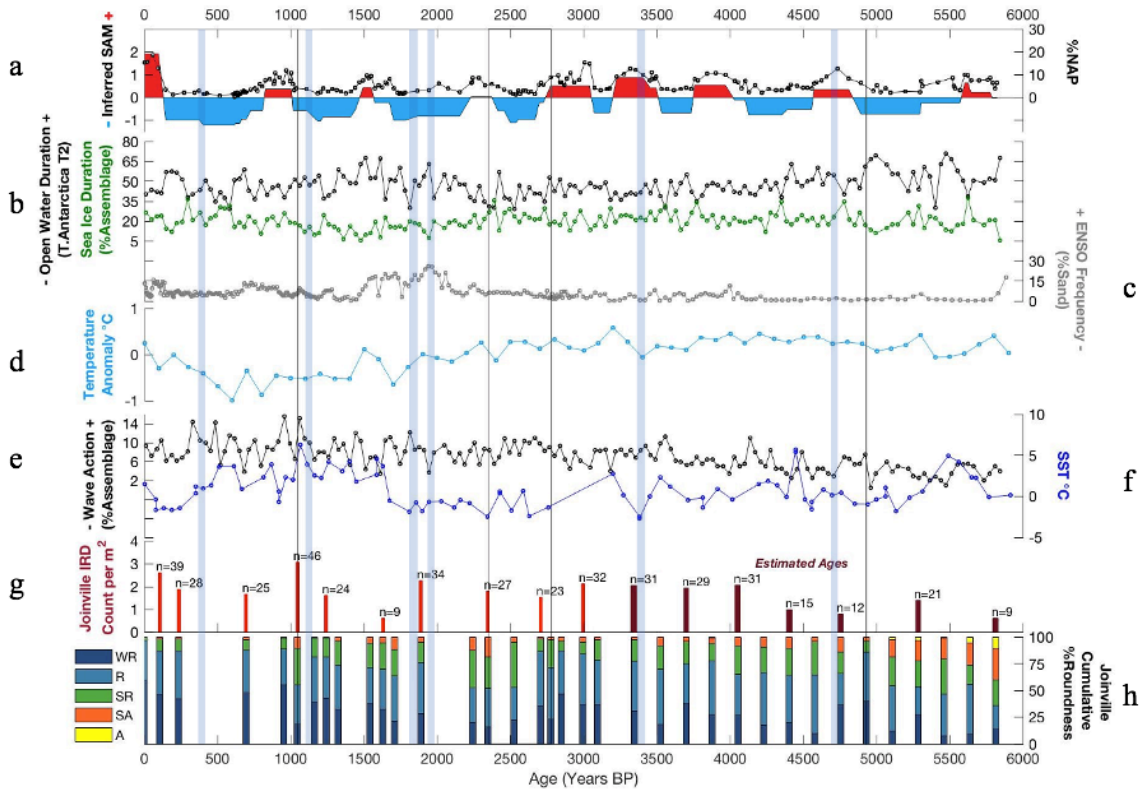

Figure 17: Chosen paleoclimate proxy records across the AP compared to the Joinville Island record. (a) Non-arboreal pollen (NAP, line) compared with regime shift detection algorithm results applied to the NAP data to infer SAM-like events (Moreno et al., 2018). Subsequently, regime shift anomalies >0 (red filling) are interpreted as positive SAM events and <0 (blue filling) are interpreted as negative SAM events. (b) Relative abundances (%) of the T. Antarctica T2 (black) and Sea Ice Assemblage (green) interpreted as a proxy for open water conditions and sea ice duration, respectively (Barbara et al., 2016). (c) Volume percent sand in a core from El Junko Crater Lake, Galapagos, interpreted as a proxy for ENSO frequency (Conroy et al., 2008). (d) Reconstructed temperature anomalies from James Ross Island (Mulvaney et al., 2012). (e) Relative abundance (%) of the benthic diatom group interpreted as a proxy for storm frequency and/or wave action (Barbara et al., 2016). (f) Palmer Deep site 1098 sea surface temperature anomalies derived from TEX86 (Shevenell et al., 2011). (g) Joinville IRD densities (n = total count) and (h) percent roundness measurements of well-rounded (WR), rounded (R), sub-rounded (SR), sub-angular (SA), and angular (A) beach materials. Beaches with anomalous rounding are indicated by thin vertical black lines. Additionally, light blue shading represents ages for Livingston Island beaches 2-7.

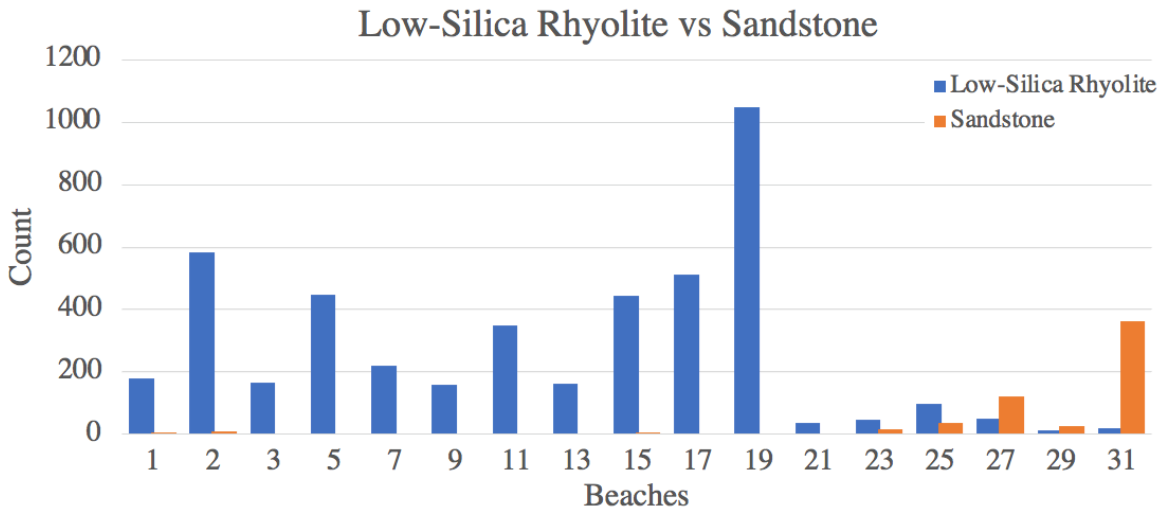

Figure 18: Image depicting the transition from sandstone to low-silica rhyolite sources for Joinville Island beaches.

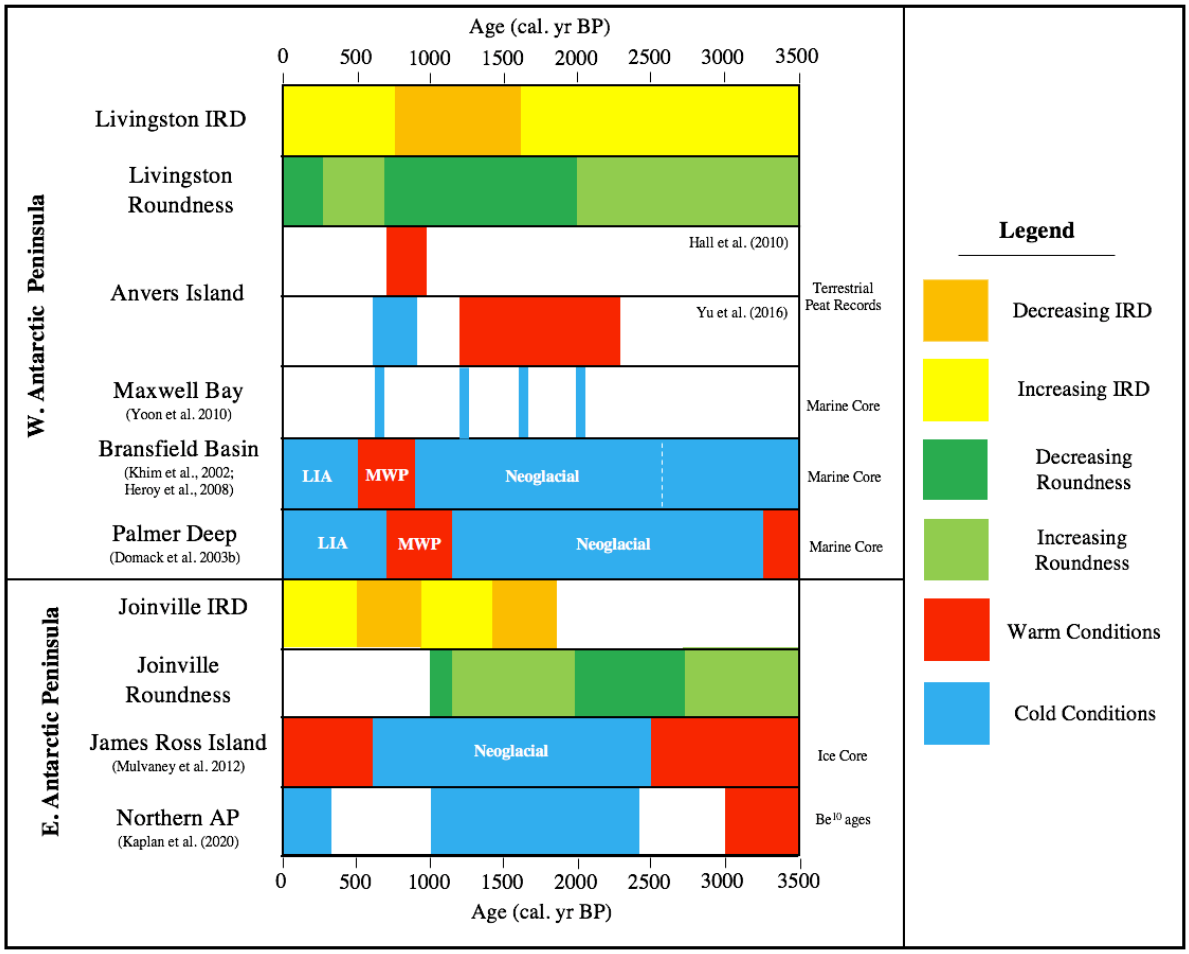

Figure 19: Chosen paleoclimate results from six records across the AP compared to the Joinville and Livingston Island IRD and roundness records. Climate periods associated with particular cooling or warming events are labeled with the name of the climate period. Non-labeled events are not associated with a particular climate period. For example, the white dashed line separates a period of increased sea ice coverage from the onset of the Neoglacial period in the Bransfield basin.

Table 1: Joinville Ages		
A: *Radiocarbon Ages*		
Beach	Age (Cal yr BP)	2σ
1	105	160
2	235	175
3	695	190
4	950	145
5	1045	135
6	1160	130
7b	1320	125
8	1540	125
9	1630	130
10	1710	135
*11	1888	150
12	2240	155
13	2345	165
15	2705	175
16	2845	155
17	2995	170
18	3095	195
*Multiple ages were given; therefore, average age was calculated		

B: *Joinville Estimated Ages*	
Beach	Estimated Age (Cal yr BP)
*7a	1240
*14	2525
*15b	2775
19	3347
20a	3523
21	3699
22	3875
23	4051
24	4227
25	4403
26	4579
27	4755
28a	4931
28b	5107
29	5283
30a	5459
30b	5635
31	5800
The average rate of beach formation used is 176 yrs.	

*Intermediate beaches that required estimation between beach ridges and do not follow the average rate of beach formation

Table 2: Livingston Ages			
A: *Radiocarbon Ages*			
Beach Name	Beach Elevation (amsl)	Age (Cal yr BP)	2σ
2	4.8	420	474
4	8.5	1840	611
5	9.7	1930	639

B: *Estimated Ages*		
Beach Name	Beach Elevation (amsl)	Age (Cal yr BP)
1 (Modern)	0.5	0
3	4.5	1130
6	9.6	3323
7	10.1	4715
8	10.1	6108
*9	12.1	7500
*Age was estimated in previous publication (Hall, 2010).		

Table 3: Joinville Island Grain-size Data			
Beach ID	**Average (cm)**	**Median (cm)**	**Standard Deviation**
Modern	3.52	3.35	1.17
1	2.94	2.80	0.98
2	3.71	3.58	1.45
3	3.51	3.38	1.10
4	3.13	2.97	1.11
5	4.03	3.97	1.01
6	3.53	3.28	1.13
7a	2.72	2.59	0.95
7b	3.19	3.01	1.07
8	2.97	2.78	1.22
9	2.70	2.35	1.17
10	2.51	2.28	1.03
11	2.53	2.27	1.11
12	2.60	2.44	1.02
13	3.07	2.82	1.30
14	2.14	1.92	0.94
15a	3.32	3.14	1.02
15b	2.57	2.53	0.91
16	2.65	2.48	0.83

17	3.16	2.99	1.06
18	3.18	2.99	1.20
19	3.81	3.60	1.30
20a	3.15	2.92	1.07
21	3.34	3.22	1.11
22	3.39	3.30	0.98
23	3.06	2.89	0.85
24	4.02	3.79	1.33
25	2.83	2.61	1.12
26	3.48	3.30	0.96
27	2.91	2.57	1.21
28a	2.85	2.70	0.95
28b	3.78	3.59	1.04
29	3.62	3.52	1.18
30a	2.03	1.88	0.92
30b	2.11	1.91	0.84
31	4.29	4.00	2.20
Island Average	3.12	2.94	1.11

Table 4: Livingston Island Grain-size Data

Beach ID	**Average (cm)**	**Median (cm)**	**Standard Deviation**
Modern	5.39	4.80	2.63
2	2.73	2.30	1.24
3	1.68	1.49	0.80
4	3.56	3.0	2.13
5	3.09	2.80	1.32
6	1.95	1.80	0.79
7	3.62	3.30	1.18
8	5.75	5.0	2.71
9	3.07	2.70	1.35
Island Average	3.43	3.02	1.57

References

Ahmed, M., Anchukaitis, K. J., Asrat, A., Borgaonkar, H. P., Braida, M., Buckley, B. M., Büntgen, U., Chase, B. M., Christie, D. A., and Cook, E. R., 2013, Continental-scale temperature variability during the past two millennia: Nature geoscience, v. 6, no. 5, p. 339-346.

Anderson, J. B., 1999, Antarctic marine geology, Cambridge University Press.

Balco, G., and Schaefer, J. M., 2013, Exposure-age record of Holocene ice sheet and ice shelf change in the northeast Antarctic Peninsula: Quaternary Science Reviews, v. 59, p. 101-111.

Barbara, L., Crosta, X., Leventer, A., Schmidt, S., Etourneau, J., Domack, E., and Massé, G., 2016, Environmental responses of the Northeast Antarctic Peninsula to the Holocene climate variability: Paleoceanography, v. 31, no. 1, p. 131-147.

Baroni, C., and Hall, B. L., 2004, A new Holocene relative sea-level curve for Terra Nova Bay, Victoria Land, Antarctica: Journal of Quaternary Science, v. 19, no. 4, p. 377-396.

Bentley, M., Hodgson, D., Smith, J., and Cox, N., 2005a, Relative sea level curves for the South Shetland Islands and Marguerite Bay, Antarctic Peninsula: Quaternary Science Reviews, v. 24, no. 10-11, p. 1203-1216.

Bentley, M., Hodgson, D., Sugden, D., Roberts, S., Smith, J., Leng, M., and Bryant, C., 2005b, Early Holocene retreat of the George VI ice shelf, Antarctic Peninsula: Geology, v. 33, no. 3, p. 173-176.

Bentley, M., Hodgson, D., Smith, J., Cofaigh, C., Domack, E., Larter, R., Roberts, S., Brachfeld, S., Leventer, A., and Hjort, C., 2009, Mechanisms of Holocene palaeoenvironmental change in the Antarctic Peninsula region: The Holocene, v. 19, no. 1, p. 51-69.

Birkenmajer, K., 1981, Pre-Quaternary fossiliferous glacio-marine deposits at Cape Melville, King George Island (South Shetland Islands, West Antarctica).

Birkenmajer, K., 1996, Glacier retreat and raised marine beaches at Three Sisters Point, King George Island (South Shetland Islands, West Antarctica): Oceanographic Literature Review, v. 5, no. 43, p. 459.

Birkenmajer, K., 1998, Quaternary geology at Potter Peninsula, King George Island (South Shetland Islands, West Antarctica): Bulletin of the Polish Academy of Sciences. Earth Sciences, v. 46, no. 1, p. 9-20.

Björck, S., Olsson, S., Ellis-Evans, C., Håkansson, H., Humlum, O., and de Lirio, J. M., 1996, Late Holocene palaeoclimatic records from lake sediments on James Ross Island, Antarctica: Palaeogeography, Palaeoclimatology, Palaeoecology, v. 121, no. 3-4, p. 195-220.

Björck, S., Hjort, C., Ingólfsson, O., Zale, R., and Ising, J., 1996, Holocene deglaciation chronology from lake sediments, Geomorphological Map of Byers Peninsula, Livingston Island. Bas Geomap Series Sheet 5-a, British Antarctic Survey, p. 49-51.

Boggs, S., 1995, Principles of sedimentology and stratigraphy, Prentice Hall New Jersey.

Bond, G., Heinrich, H., Broecker, W., Labeyrie, L., McManus, J., Andrews, J., Huon, S., Jantschik, R., Clasen, S., and Simet, C., 1992, Evidence for massive discharges of icebergs into the North Atlantic ocean during the last glacial period: Nature, v. 360, no. 6401, p. 245.

Brachfeld, S., Domack, E., Kissel, C., Laj, C., Leventer, A., Ishman, S., Gilbert, R., Camerlenghi, A., and Eglinton, L. B., 2003, Holocene history of the Larsen-A Ice Shelf constrained by geomagnetic paleointensity dating: Geology, v. 31, no. 9, p. 749-752.

Butler, E. R., 1999, Process environments on modern and raised beaches in McMurdo Sound, Antarctica: Marine Geology, v. 162, no. 1, p. 105-120.

Bøtter-Jensen, L., 1997, Luminescence techniques: instrumentation and methods: Radiation Measurements, v. 27, no. 5-6, p. 749-768.

Bøtter-Jensen, L., and Murray, A., 2001, Optically stimulated luminescence techniques in retrospective dosimetry: Radiation Physics and Chemistry, v. 61, no. 3-6, p. 181-190.

Carter, R., and Orford, J., 1984, Coarse clastic barrier beaches: a discussion of the distinctive dynamic and morphosedimentary characteristics: Marine Geology, v. 60, no. 1-4, p. 377-389.

Clark, P. U., Mitrovica, J., Milne, G., and Tamisiea, M., 2002, Sea-level fingerprinting as a direct test for the source of global meltwater pulse IA: Science, v. 295, no. 5564, p. 2438-2441.

Conroy, J. L., Overpeck, J. T., Cole, J. E., Shanahan, T. M., and Steinitz-Kannan, M., 2008, Holocene changes in eastern tropical Pacific climate inferred from a Galápagos lake sediment record: Quaternary Science Reviews, v. 27, no. 11-12, p. 1166-1180.

Curl, J. E., 1980, A glacial history of the South Shetland Islands, Antarctica: Institute of Polar Studies, The Ohio State University.

Davies, B. J., Golledge, N. R., Glasser, N. F., Carrivick, J. L., Ligtenberg, S. R., Barrand, N. E., Van Den Broeke, M. R., Hambrey, M. J., and Smellie, J. L., 2014, Modelled glacier response to centennial temperature and precipitation trends on the Antarctic Peninsula: Nature Climate Change, v. 4, no. 11, p. 993-998.

Davies, J., 1964, A morphogenic approach to world shorelines: Zeitschrift fur Geomorphologie, v. 8, p. 127-142.

Domack, E. W., A synthesis for site 1098: Palmer Deep, *in* Proceedings Proceedings of the Ocean Drilling Program, scientific results2002, Volume 178, Ocean Drilling Program, Texas A&M University, College Station TX, p. 77843-79547.

Domack, E. W., Duran, D., Leventer, A., Ishman, S., Doane, S., McCallum, S., Amblas, D., Ring, J., Gilbert, R., and Prentice, M., 2005, Stability of the Larsen B ice shelf on the Antarctic Peninsula during the Holocene epoch: Nature, v. 436, no. 7051, p. 681.

Domack, E. W., Leventer, A., Dunbar, R., Taylor, F., Brachfeld, S., and Sjunneskog, C., 2001, Chronology of the Palmer Deep site, Antarctic Peninsula: a Holocene palaeoenvironmental reference for the circum-Antarctic: The Holocene, v. 11, no. 1, p. 1-9.

Domack, E. W., Burnett, A., and Leventer, A., 2003a, Environmental setting of the Antarctic Peninsula: Antarctic Peninsula climate variability: historical and paleoenvironmental perspectives, v. 79, p. 1-13.

Domack, E. W., Ishman, S. E., Stein, A. B., McClennen, C. E., and Jull, A. T., 1995, Late Holocene advance of the Müller Ice Shelf, Antarctic Peninsula: sedimentological, geochemical and palaeontological evidence: Antarctic Science, v. 7, no. 2, p. 159-170.

Domack, E. W., Leventer, A., Root, S., Ring, J., Williams, E., Carlson, D., Hirshorn, E., Wright, W., Gilbert, R., and Burr, G., 2003b, Marine sedimentary record of natural

environmental variability and recent warming in the Antarctic Peninsula: Antarctic peninsula climate variability: Historical and paleoenvironmental perspectives, v. 79, p. 205-224.
Domack, E. W., and Mcclennen, C. E., 1996, Accumulation of glacial marine sediments in fjords of the Antarctic Peninsula and their use as late Holocene paleoenvironmental indicators: Foundations for ecological research west of the Antarctic Peninsula, v. 70, p. 135-154.
Dominguez, J. M., Andrade, A. C., Almeida, A. B., and Bittencourt, A. C., 2009, The Holocene barrier strandplains of the state of Bahia, Geology and Geomorphology of Holocene coastal barriers of Brazil, Springer, p. 253-288.
Elliot, D., 1967, The geology of joinville island: British Antarctic Survey Bulletin, v. 12, p. 23-40.
Evans, D., Lautenbacher, C., Spinrad, R., and Szabados, M., 2003, Computational techniques for tidal datums handbook: NOAA Special Publication NOS CO-OPS, v. 2.
Evans, J., Pudsey, C. J., ÓCofaigh, C., Morris, P., and Domack, E., 2005, Late Quaternary glacial history, flow dynamics and sedimentation along the eastern margin of the Antarctic Peninsula Ice Sheet: Quaternary Science Reviews, v. 24, no. 5-6, p. 741-774.
Forbes, D., Orford, J., Carter, R., Shaw, J., and Jennings, S., 1995, Morphodynamic evolution, self-organisation, and instability of coarse-clastic barriers on paraglacial coasts: Marine Geology, v. 126, no. 1-4, p. 63-85.
Forrest, B. M., 2007, Evolution of the beach ridge strandplain on St. Vincent Island, Florida.
Fretwell, P. T., Hodgson, D., Watcham, E., Bentley, M., and Roberts, S. J., 2010, Holocene isostatic uplift of the South Shetland Islands, Antarctic Peninsula, modelled from raised beaches: Quaternary Science Reviews, v. 29, no. 15-16, p. 1880-1893.
Garcıa, M., Castro, C. G., Rıos, A., Doval, M. D., Rosón, G., Gomis, D., and López, O., 2002, Water masses and distribution of physico-chemical properties in the Western Bransfield Strait and Gerlache Strait during Austral summer 1995/96: Deep Sea Research Part II: Topical Studies in Oceanography, v. 49, no. 4-5, p. 585-602.
Gardner, N., Hall, B., and Wehmiller, J., 2006, Pre-Holocene raised beaches at Cape Ross, Southern Victoria Land, Antarctica: Marine Geology, v. 229, no. 3-4, p. 273-284.
Gernant, C., Simms, A., DeWitt, R., Garcia, C., and Theilen, B., 2020, Insights into the sea-level history of the South Shetland Islands from ground penetrating radar on Livingston Island, Antarctica: Abstract 58-10 presented at 2020 annual meeting, GSA 2020 Connects Online: Montréal, Quebec, 25-28 October.
Guglielmin, M., Convey, P., Malfasi, F., and Cannone, N., 2016, Glacial fluctuations since the 'Medieval warm period'at Rothera Point (western Antarctic Peninsula): The Holocene, v. 26, no. 1, p. 154-158.
Hall, B., 2010, Holocene relative sea-level changes and ice fluctuations in the South Shetland Islands: Global and Planetary Change, v. 74, no. 1, p. 15-26.
Hall, B., Koffman, T., and Denton, G., 2010a, Reduced ice extent on the western Antarctic Peninsula at 700–970 cal. yr BP: Geology, v. 38, no. 7, p. 635-638.
Hall, B., 2003, An overview of late Pleistocene glaciation in the South Shetland Islands: Antarctic Research Series, v. 79, p. 103-113.
Hall, B., 2007, Late-Holocene advance of the Collins Ice Cap, King George Island, South Shetland Islands: The Holocene, v. 17, no. 8, p. 1253-1258.

Hall, B., 2009, Holocene glacial history of Antarctica and the sub-Antarctic islands: Quaternary Science Reviews, v. 28, no. 21-22, p. 2213-2230.
Hall, B., Henderson, G. M., Baroni, C., and Kellogg, T. B., 2010b, Constant Holocene Southern-Ocean 14C reservoir ages and ice-shelf flow rates: Earth and Planetary Science Letters, v. 296, no. 1-2, p. 115-123.
Hall, B., and Perry, E. R., 2004, Variations in ice rafted detritus on beaches in the South Shetland Islands: a possible climate proxy: Antarctic Science, v. 16, no. 3, p. 339-344.
Hansom, J., 1979, Radiocarbon dating of a raised beach at 10 m in the South Shetland Islands: British Antarctic Survey Bulletin, v. 49, p. 287-288.
Hobbs, G., 1968, The geology of the South Shetland Islands: IV. The geology of Livingston Island, British Antarctic Survey.
Hodgson, D. A., and Convey, P., 2005, A 7000-year record of oribatid mite communities on a maritime-Antarctic island: responses to climate change: Arctic, Antarctic, and Alpine Research, v. 37, no. 2, p. 239-245.
Hodgson, D. A., Doran, P. T., Roberts, D., and McMinn, A., 2004, Paleolimnological studies from the Antarctic and subantarctic islands, Long-term environmental change in Arctic and Antarctic lakes, Springer, p. 419-474.
Hofmann, E. E., Klinck, J. M., Lascara, C. M., and Smith, D. A., 1996, Water mass distribution and circulation west of the Antarctic Peninsula and including Bransfield Strait: Foundations for ecological research west of the Antarctic Peninsula, v. 70, p. 61-80.
Hong, S., Lee, M. K., Seong, Y. B., Owen, L. A., Rhee, H. H., Lee, J. I., and Yoo, K.-C., 2020, Holocene sea-level history and tectonic implications derived from luminescence dating of raised beaches in Terra Nova Bay, Antarctica: Geosciences Journal, p. 1-16.
Houghton, J., 2001, Climate Change 2001: The Scientific Basis.
Ingólfsson, Ó., Hjort, C., and Humlum, O., 2003, Glacial and climate history of the Antarctic Peninsula since the Last Glacial Maximum: Arctic, Antarctic, and Alpine Research, v. 35, no. 2, p. 175-186.
John, B., and Sugden, D., 1971, Raised marine features and phases of glaciation in the South Shetland Islands: British Antarctic Survey Bulletin, v. 24, p. 45-111.
Kaminuma, K., 1995, Seismicity around the Antarctic Peninsula.
Kanfoush, S. L., Hodell, D. A., Charles, C. D., Janecek, T. R., and Rack, F. R., 2002, Comparison of ice-rafted debris and physical properties in ODP Site 1094 (South Atlantic) with the Vostok ice core over the last four climatic cycles: Palaeogeography, Palaeoclimatology, Palaeoecology, v. 182, no. 3-4, p. 329-349.
Kaplan, M., Strelin, J., Schaefer, J., Peltier, C., Martini, M., Flores, E., Winckler, G., and Schwartz, R., 2020, Holocene glacier behavior around the northern Antarctic Peninsula and possible causes: Earth and Planetary Science Letters, v. 534, p. 116077.
Khim, B.-K., Yoon, H. I., Kang, C. Y., and Bahk, J. J., 2002, Unstable climate oscillations during the late Holocene in the eastern Bransfield Basin, Antarctic Peninsula: Quaternary Research, v. 58, no. 3, p. 234-245.

Kulbe, T., Melles, M., Verkulich, S. R., and Pushina, Z. V., 2001, East Antarctic climate and environmental variability over the last 9400 years inferred from marine sediments of the Bunger Oasis: Arctic, Antarctic, and Alpine Research, v. 33, no. 2, p. 223-230.
Kwok, R., and Comiso, J. C., 2002, Spatial patterns of variability in Antarctic surface temperature: Connections to the Southern Hemisphere Annular Mode and the Southern Oscillation: Geophysical Research Letters, v. 29, no. 14, p. 50-51-50-54.
Lambeck, K., 1993, Glacial rebound and sea-level change: an example of a relationship between mantle and surface processes: Tectonophysics, v. 223, no. 1-2, p. 15-37.
Lindhorst, S., and Schutter, I., 2014, Polar gravel beach-ridge systems: Sedimentary architecture, genesis, and implications for climate reconstructions (South Shetland Islands/Western Antarctic Peninsula): Geomorphology, v. 221, p. 187-203.
Lopez-Martinez, J., Thomson, M., Arche, A., Bjorck, S., Ellis-Evans, J. C., Hatway, B., Hernández-Cifuentes, F., Hjort, C., Ingolfsson, O., and Ising, J., 1996, geomorphological map of Byers peninsula, livingston island.
Manabe, S., and Stouffer, R. J., 1997, Coupled ocean-atmosphere model response to freshwater input: Comparison to Younger Dryas event: Paleoceanography, v. 12, no. 2, p. 321-336.
Masson-Delmotte, V., Stenni, B., and Jouzel, J., 2004, Common millennial-scale variability of Antarctic and Southern Ocean temperatures during the past 5000 years reconstructed from the EPICA Dome C ice core: The Holocene, v. 14, no. 2, p. 145-151.
Matsumoto, K., 1996, An iceberg drift and decay model to compute the ice-rafted debris and iceberg meltwater flux: Application to the interglacial North Atlantic: Paleoceanography, v. 11, no. 6, p. 729-742.
Michalchuk, B. R., Anderson, J. B., Wellner, J. S., Manley, P. L., Majewski, W., and Bohaty, S., 2009, Holocene climate and glacial history of the northeastern Antarctic Peninsula: the marine sedimentary record from a long SHALDRIL core: Quaternary Science Reviews, v. 28, no. 27-28, p. 3049-3065.
Milliken, K., Anderson, J., Wellner, J., Bohaty, S., and Manley, P., 2009, High-resolution Holocene climate record from Maxwell Bay, South Shetland Islands, AntarcticaHolocene climate record from Maxwell Bay: GSA Bulletin, v. 121, no. 11-12, p. 1711-1725.
Minzoni, R. T., Anderson, J. B., Fernandez, R., and Wellner, J. S., 2015, Marine record of Holocene climate, ocean, and cryosphere interactions: herbert sound, James Ross island, Antarctica: Quaternary Science Reviews, v. 129, p. 239-259.
Moreno, P., Vilanova, I., Villa-Martínez, R., Dunbar, R., Mucciarone, D., Kaplan, M., Garreaud, R., Rojas, M., Moy, C., and De Pol-Holz, R., 2018, Onset and evolution of southern annular mode-like changes at centennial timescale: Scientific reports, v. 8, no. 1, p. 1-9.
Mulvaney, R., Abram, N. J., Hindmarsh, R. C., Arrowsmith, C., Fleet, L., Triest, J., Sime, L. C., Alemany, O., and Foord, S., 2012, Recent Antarctic Peninsula warming relative to Holocene climate and ice-shelf history: Nature, v. 489, no. 7414, p. 141.
Murray, A. S., and Olley, J. M., 2002, Precision and accuracy in the optically stimulated luminescence dating of sedimentary quartz: a status review: Geochronometria, v. 21, no. 1, p. 1-16.

Murray, A. S., and Wintle, A. G., 2000, Luminescence dating of quartz using an improved single-aliquot regenerative-dose protocol: Radiation measurements, v. 32, no. 1, p. 57-73.
Nichols, R. L., 1961, Characteristics of beaches formed in polar climates: American Journal of Science, v. 259, no. 9, p. 694-708.
Nield, G. A., Barletta, V. R., Bordoni, A., King, M. A., Whitehouse, P. L., Clarke, P. J., Domack, E., Scambos, T. A., and Berthier, E., 2014, Rapid bedrock uplift in the Antarctic Peninsula explained by viscoelastic response to recent ice unloading: Earth and Planetary Science Letters, v. 397, p. 32-41.
Orsi, A. H., Nowlin Jr, W. D., and Whitworth III, T., 1990, On the circulation and stratification of the Weddell Gyre: Texas A&M University.
Palacios, D., Ruiz-Fernández, J., Oliva, M., Andrés, N., Fernández-Fernández, J. M., Schimmelpfennig, I., Leanni, L., González-Díaz, B., and Team, A., 2020, Timing of formation of neoglacial landforms in the South Shetland Islands (Antarctic Peninsula): Regional and global implications: Quaternary Science Reviews, v. 234, p. 106248.
Powers, M. C., 1953, A new roundness scale for sedimentary particles: Journal of Sedimentary Research, v. 23, no. 2, p. 117-119.
Pudsey, C., Barker, P., and Larter, R., 1994, Ice sheet retreat from the Antarctic Peninsula shelf: Continental Shelf Research, v. 14, no. 15, p. 1647-1675.
Pudsey, C., Murray, J. W., Appleby, P., and Evans, J., 2006, Ice shelf history from petrographic and foraminiferal evidence, Northeast Antarctic Peninsula: Quaternary Science Reviews, v. 25, no. 17-18, p. 2357-2379.
Reimer, P. J., Bard, E., Bayliss, A., Beck, J. W., Blackwell, P. G., Ramsey, C. B., Buck, C. E., Cheng, H., Edwards, R. L., and Friedrich, M., 2013, IntCal13 and Marine13 radiocarbon age calibration curves 0–50,000 years cal BP: Radiocarbon, v. 55, no. 4, p. 1869-1887.
Reynolds, J. M., and JM, R., 1981, The distribution of mean annual temperatures in the Antarctic Peninsula.
Roberts, S., Hodgson, D., Bentley, M., Sanderson, D., Milne, G., Smith, J., Verleyen, E., and Balbo, A., 2009, Holocene relative sea-level change and deglaciation on Alexander Island, Antarctic Peninsula, from elevated lake deltas: Geomorphology, v. 112, no. 1-2, p. 122-134.
Roberts, S., Hodgson, D. A., Sterken, M., Whitehouse, P. L., Verleyen, E., Vyverman, W., Sabbe, K., Balbo, A., Bentley, M. J., and Moreton, S. G., 2011, Geological constraints on glacio-isostatic adjustment models of relative sea-level change during deglaciation of Prince Gustav Channel, Antarctic Peninsula: Quaternary Science Reviews, v. 30, no. 25-26, p. 3603-3617.
Scheffers, A., Engel, M., Scheffers, S., Squire, P., and Kelletat, D., 2012, Beach ridge systems–archives for Holocene coastal events?: Progress in Physical Geography, v. 36, no. 1, p. 5-37.
Shevenell, A., Ingalls, A., Domack, E., and Kelly, C., 2011, Holocene Southern Ocean surface temperature variability west of the Antarctic Peninsula: Nature, v. 470, no. 7333, p. 250.

Shevenell, A., and Kennett, J. P., 2002, Antarctic Holocene climate change: A benthic foraminiferal stable isotope record from Palmer Deep: Paleoceanography, v. 17, no. 2, p. PAL 9-1-PAL 9-12.
Shindell, D. T., and Schmidt, G. A., 2004, Southern Hemisphere climate response to ozone changes and greenhouse gas increases: Geophysical Research Letters, v. 31, no. 18.
Simkins, L. M., DeWitt, R., Simms, A. R., Briggs, S., and Shapiro, R. S., 2016, Investigation of optically stimulated luminescence behavior of quartz from crystalline rock surfaces: A look forward: Quaternary Geochronology, v. 36, p. 161-173.
Simkins, L. M., Simms, A. R., and DeWitt, R., 2013, Relative sea-level history of Marguerite Bay, Antarctic Peninsula derived from optically stimulated luminescence-dated beach cobbles: Quaternary Science Reviews, v. 77, p. 141-155.
Simkins, L. M., 2015, Assessing the link between coastal morphology, wave energy and sea ice throughout the Holocene from Antarctic raised beaches: Journal of Quaternary Science, v. 30, no. 4, p. 335-348.
Simms, A. R, Whitehouse, P., Simkins, L., Nield, G., DeWitt, R., and Bentley, M., 2018, Late Holocene relative sea-level reconstruction near Palmer Station, northern Antarctic Peninsula may record Late Holocene ice mass changes not LGM glacial isostatic adjustment: Quaternary science reviews.
Simms, A. R., DeWitt, R., Kouremenos, P., and Drewry, A. M., 2011, A new approach to reconstructing sea levels in Antarctica using optically stimulated luminescence of cobble surfaces: Quaternary Geochronology, v. 6, no. 1, p. 50-60.
Simms, A. R., Ivins, E. R., DeWitt, R., Kouremenos, P., and Simkins, L. M., 2012, Timing of the most recent Neoglacial advance and retreat in the South Shetland Islands, Antarctic Peninsula: insights from raised beaches and Holocene uplift rates: Quaternary Science Reviews, v. 47, p. 41-55.
Singhvi, A., Stokes, S., Chauhan, N., Nagar, Y., and Jaiswal, M., 2011, Changes in natural OSL sensitivity during single aliquot regeneration procedure and their implications for equivalent dose determination: Geochronometria, v. 38, no. 3, p. 231-241.
Smith, J. A., Bentley, M. J., Hodgson, D. A., Roberts, S. J., Leng, M. J., Lloyd, J. M., Barrett, M. S., Bryant, C., and Sugden, D. E., 2007, Oceanic and atmospheric forcing of early Holocene ice shelf retreat, George VI Ice Shelf, Antarctica Peninsula: Quaternary Science Reviews, v. 26, no. 3-4, p. 500-516.
Stammerjohn, S., and Smith, R., 1996, Spatial and temporal variability of western Antarctic Peninsula sea ice coverage: Foundations for ecological research west of the Antarctic Peninsula, v. 70, p. 81-104.
Stammerjohn, S. E., Martinson, D., Smith, R., Yuan, X., and Rind, D., 2008, Trends in Antarctic annual sea ice retreat and advance and their relation to El Niño–Southern Oscillation and Southern Annular Mode variability: Journal of Geophysical Research: Oceans, v. 113, no. C3.
Sterken, M., Roberts, S. J., Hodgson, D. A., Vyverman, W., Balbo, A. L., Sabbe, K., Moreton, S. G., and Verleyen, E., 2012, Holocene glacial and climate history of Prince Gustav Channel, northeastern Antarctic Peninsula: Quaternary science reviews, v. 31, p. 93-111.
Stuiver, M., and Reimer, P. J., 1993, Extended 14 C data base and revised CALIB 3.0 14 C age calibration program: Radiocarbon, v. 35, no. 1, p. 215-230.

Stuiver, M., Reimer, P. J., and Braziunas, T. F., 1998, High-precision radiocarbon age calibration for terrestrial and marine samples: radiocarbon, v. 40, no. 3, p. 1127-1151.
Tamura, T., 2012, Beach ridges and prograded beach deposits as palaeoenvironment records: Earth-Science Reviews, v. 114, no. 3-4, p. 279-297.
Vaughan, D. G., Marshall, G. J., Connolley, W. M., Parkinson, C., Mulvaney, R., Hodgson, D. A., King, J. C., Pudsey, C. J., and Turner, J., 2003, Recent rapid regional climate warming on the Antarctic Peninsula: Climatic change, v. 60, no. 3, p. 243-274.
Watcham, E., Bentley, M., Hodgson, D., Roberts, S. J., Fretwell, P., Lloyd, J., Larter, R., Whitehouse, P., Leng, M., and Monien, P., 2011, A new Holocene relative sea level curve for the South Shetland Islands, Antarctica: Quaternary Science Reviews, v. 30, no. 21, p. 3152-3170.
Whitehouse, P. L., 2018, Glacial isostatic adjustment modelling: historical perspectives, recent advances, and future directions: Earth surface dynamics., v. 6, no. 2, p. 401-429.
Yoon, H. I., Yoo, K.-C., Bak, Y.-S., Lim, H. S., Kim, Y., and Lee, J. I., 2010, Late Holocene cyclic glaciomarine sedimentation in a subpolar fjord of the South Shetland Islands, Antarctica, and its paleoceanographic significance: Sedimentological, geochemical, and paleontological evidence: Bulletin, v. 122, no. 7-8, p. 1298-1307.
Yu, Z., Beilman, D. W., and Loisel, J., 2016, Transformations of landscape and peat-forming ecosystems in response to late Holocene climate change in the western Antarctic Peninsula: Geophysical Research Letters, v. 43, no. 13, p. 7186-7195.
Yuan, X., 2004, ENSO-related impacts on Antarctic sea ice: a synthesis of phenomenon and mechanisms: Antarctic Science, v. 16, no. 4, p. 415-425.
Zurbuchen, J., and Simms, A. R., 2019, Late Holocene ice-mass changes recorded in a relative sea-level record from Joinville Island, Antarctica: Geology.

Appendix A. Supplementary Files

Complete grain size, roundness, and ice rafted debris data can be found here:
https://doi.org/10.15784/601400

LIST OF FIGURES

LIST OF TABLES

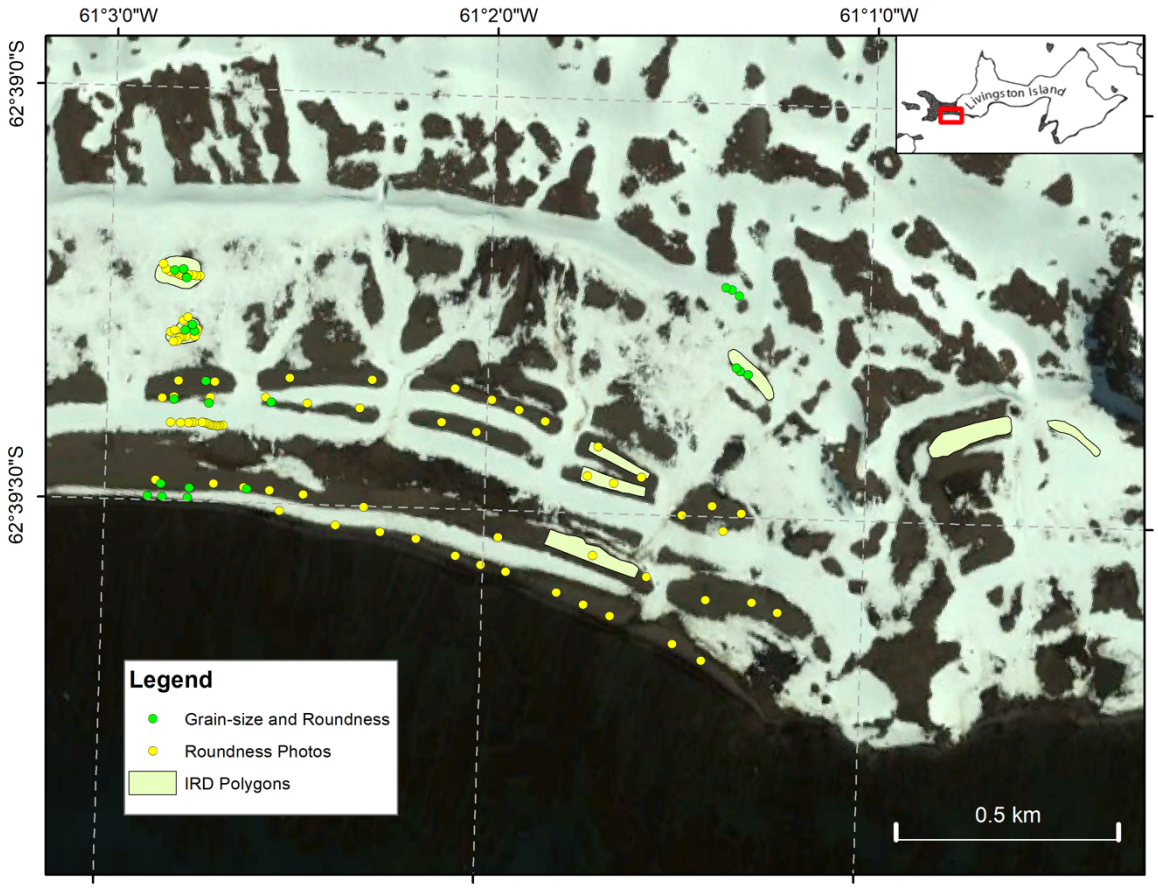

Figure A1: Map of Livingston Island grain size and roundness sample locations and IRD observations.

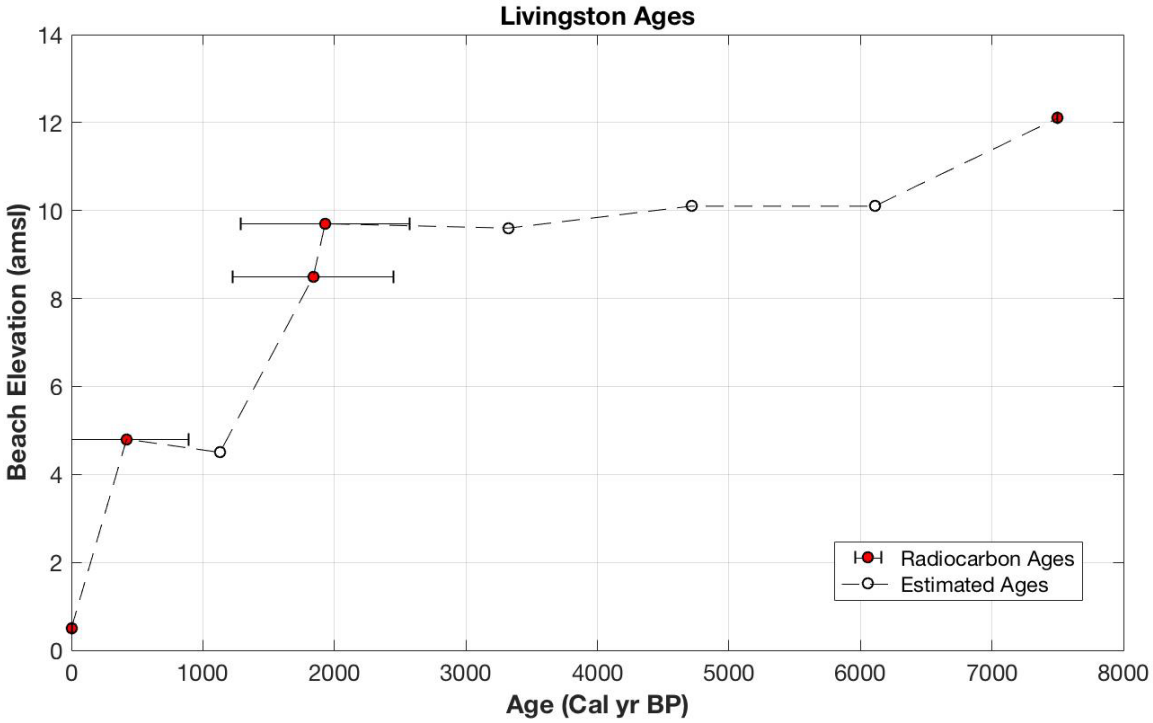

Figure A2: Livingston Island beach ages compared to elevations above mean sea level. Beach ridge radiocarbon ages are displayed as filled circles with 2 standard deviation error bars, except for beach 9.

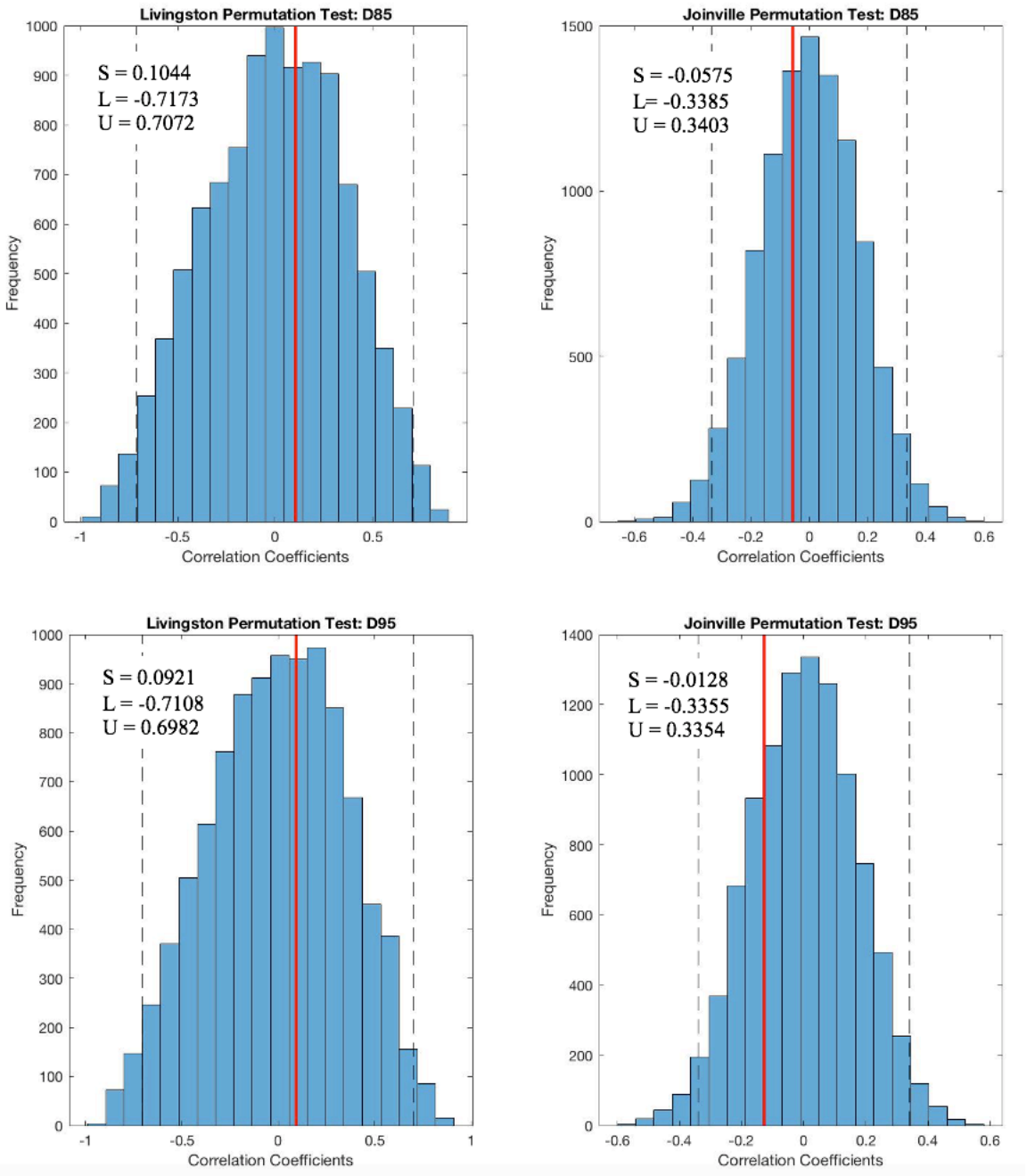

Figure A3: Permutation significance test results for the sample correlation coefficients between average roundness and average D95 and D85 grain sizes. Each permutation test was performed using 10,000 iterations of permuted pairs. The red lines depicted in each graph are the sample correlation coefficients (S) and the dashed lines are the upper (U) and lower (L) bounds of the 95% confidence interval. Each sample correlation coefficient remains within the 95% confidence interval, indicating the grain size and roundness data are uncorrelated.

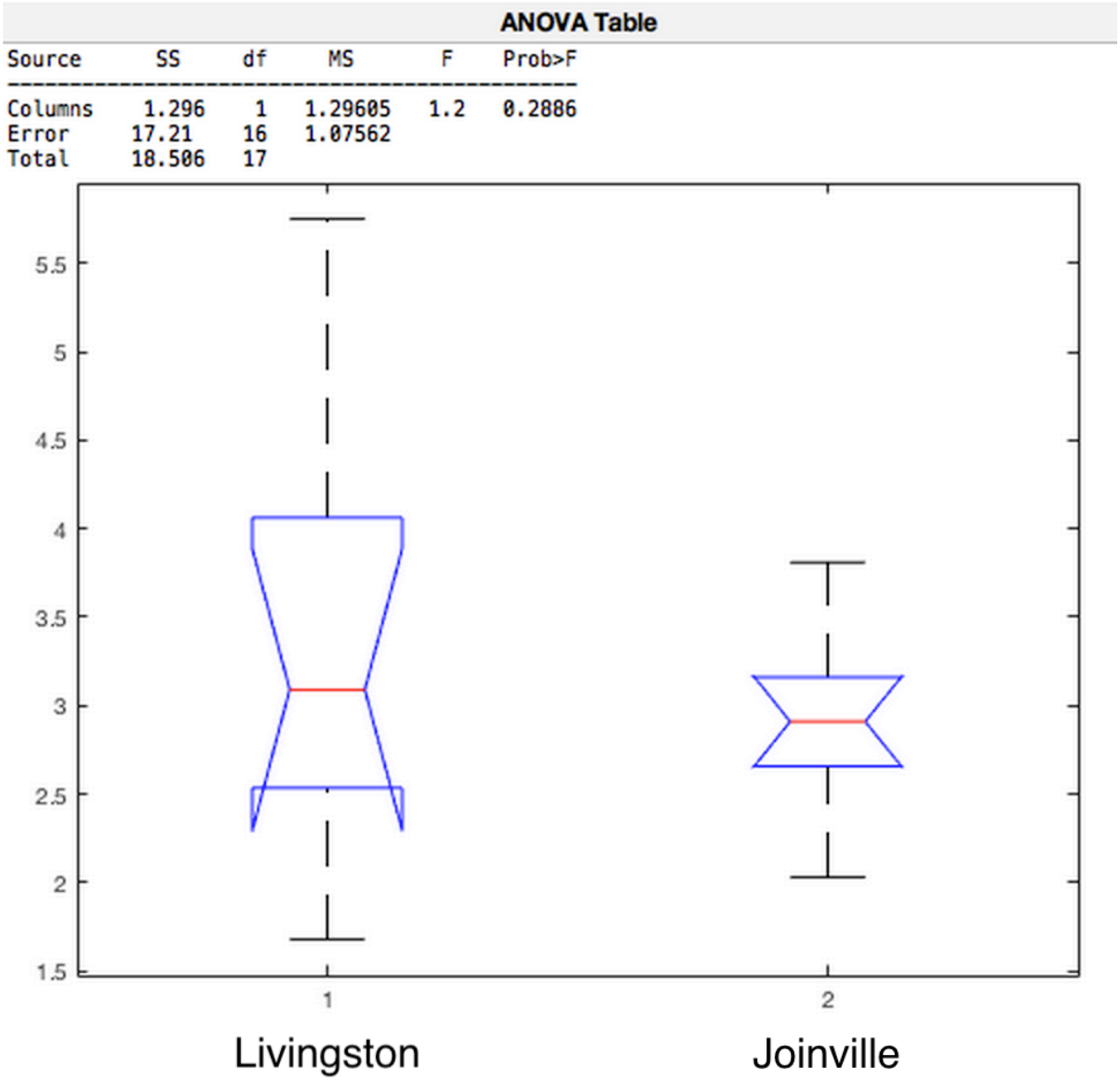

Figure A4: One-way analysis of variance (ANOVA) test results for Livingston and Joinville Islands average grain size. One-way ANOVA determines whether data from different groups have a common mean. Thus, the large p-value (0.2886) cannot reject the null hypothesis that the variances in average grain sizes are equal across islands with a 95% confidence.

Group Summary Table

Group	Count	Mean	Std Dev
1	9	1.57222	0.73399
2	9	1.11333	0.1258
Pooled	18	1.34278	0.52658

Levene's statistic (quadratic)	8.96763
Degrees of freedom	1, 16
p-value	0.00858

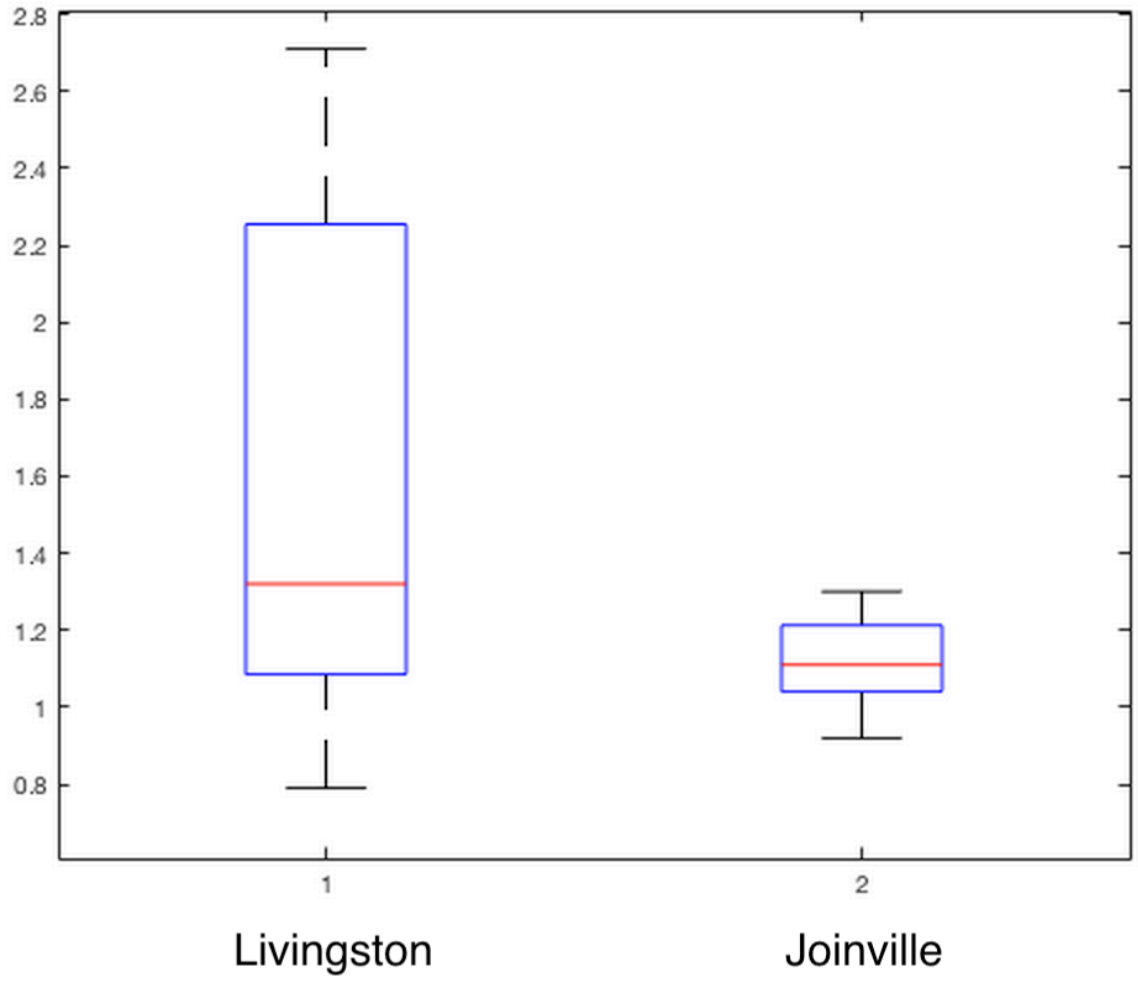

Figure A5: Levene's test results for Livingston and Joinville Island's overall standard deviations. Levene's test (quadratic) is computed by performing ANOVA on the squared deviations of the data values from their group means. Thus, the small p-value (0.0086) rejects the null hypothesis that the variances in standard deviation are equal across islands with a 95% confidence.

Table A1: Identification of most prominent Joinville IRD (i.e. total counts >10)	
Thin Section ID	**Lithology**
JV_IRD1	Biotite Granite
JV_IRD4	Veined Chert
JV_IRD5	Polymictic Conglomerate
JV_IRD8	Veined Phyllite
JV_D01	Hornblende-Biotite Granite
JV_D02	Altered Diorite or Microdiorite
JV_SG	Microdiorite
JV_UnkE	Veined Chert
JV_UnkGrn	Veined Chert
JV_UnkB (local rock)	Medium-grained feldspathic Sandstone
BT01 (local rock)	Low-Silica Rhyolite

Table A2: Compiled Radiocarbon Ages from the South Shetland Islands		
^{14}C yr BP (1s)	Cal. yr BP (2s)	Elevation (m)
1545 +/- 46	378 +/- 510	4
1715 +/- 42	528 +/- 437	4
1461 +/- 42	303 +/- 455	5
1543 +/- 53	375 +/- 519	5
1545 +/- 41	378 +/- 504	5
1576 +/- 51	404 +/- 499	5
1625 +/- 42	448 +/- 444	5
1627 +/- 68	448 +/- 490	5
1572 +/- 42	401 +/- 489	6
1692 +/- 42	509 +/- 429	6
1622 +/- 42	445 +/- 441	7
3115 +/- 47	1948 +/- 641	9
3121 +/- 35	1956 +/- 623	10.1
2823 +/- 40	1605 +/-569	10.3
3085 +/- 39	1911 +/- 644	12
3116 +/- 40	1950 +/- 633	12
N/A	~7500	18-21

Table A3: Standard Deviation of Livingston Island roundness measurements		
Beach ID	**Standard Deviation** (with field measurements)	**Standard Deviation** (without field measurements)
1	0.069	0.054
2	0.051	0.053
3	0.059	0.059
4	0.077	0.080
5	0.092	0.095
6	0.082	0.074
7	0.10	0.10
8	0.15	0.081